Temperature trends during the Present and Last Interglacial periods — a multi-model-data comparison

P. Bakker [a, *], V. Masson-Delmotte [b], B. Martrat [c], S. Charbit [b], H. Renssen [a], M. Gröger [d, 1],
U. Krebs-Kanzow [e], G. Lohman [f], D.J. Lunt [g], M. Pfeiffer [f], S.J. Phipps [h], M. Prange [i],
S.P. Ritz [j], M. Schulz [i], B. Stenni [k], E.J. Stone [g], V. Varma [i]

[a] VU University Amsterdam, Department of Earth Sciences, Faculty of Earth and Life Sciences, Amsterdam, Netherlands
[b] Laboratoire des Sciences du Climat et de l'Environnement (IPSL/CEA-CNRS-UVSQ, UMR 8212), Gif-sur-Yvette, France
[c] Department of Environmental Chemistry, Institute of Environmental Assessment and Water Research, Spanish Council for Scientific Research, Barcelona, Spain
[d] Max Planck Institute for Meteorology, Bundesstrasse 53, 20146 Hamburg, Germany
[e] Department of Geology, Kiel University, Kiel, Germany
[f] Alfred Wegener Institute for Polar and Marine Research, Germany
[g] Bristol Research Initiative for the Dynamic Global Environment (BRIDGE), School of Geographical Sciences, University of Bristol, Bristol BS8 1SS, UK
[h] ARC Centre of Excellence for Climate System Science and Climate Change Research Centre, University of New South Wales, Sydney, Australia
[i] MARUM — Center for Marine Environmental Sciences and Faculty of Geosciences, University of Bremen, Klagenfurter Strasse, 28334 Bremen, Germany
[j] Climate and Environmental Physics, Physics Institute, and Oeschger Centre for Climate Change Research, University of Bern, Bern, Switzerland
[k] University of Trieste, Dept. of Mathematics and Geosciences, Weiss 2, 34128 Trieste, Italy

ARTICLE INFO

ABSTRACT

Though primarily driven by insolation changes associated with well-known variations in Earth's astronomical parameters, the response of the climate system during interglacials includes a diversity of feedbacks involving the atmosphere, ocean, sea ice, vegetation and land ice. A thorough multi-model-data comparison is essential to assess the ability of climate models to resolve interglacial temperature trends and to help in understanding the recorded climatic signal and the underlying climate dynamics. We present the first multi-model-data comparison of transient millennial-scale temperature changes through two intervals of the Present Interglacial (PIG; 8–1.2 ka) and the Last Interglacial (LIG; 123–116.2 ka) periods. We include temperature trends simulated by 9 different climate models, alkenone-based temperature reconstructions from 117 globally distributed locations (about 45% of them within the LIG) and 12 ice-core-based temperature trends from Greenland and Antarctica (50% of them within the LIG). The definitions of these specific interglacial intervals enable a consistent inter-comparison of the two intervals because both are characterised by minor changes in atmospheric greenhouse gas concentrations and more importantly by insolation trends that show clear similarities.

Our analysis shows that in general the reconstructed PIG and LIG Northern Hemisphere mid-to-high latitude cooling compares well with multi-model, mean-temperature trends for the warmest months and that these cooling trends reflect a linear response to the warmest-month insolation decrease over the interglacial intervals. The most notable exception is the strong LIG cooling trend reconstructed from Greenland ice cores that is not simulated by any of the models. A striking model-data mismatch is found for both the PIG and the LIG over large parts of the mid-to-high latitudes of the Southern Hemisphere where the data depicts negative temperature trends that are not in agreement with near zero trends in the simulations. In this area, the positive local summer insolation trend is counteracted in climate models by an enhancement of the Southern Ocean summer sea-ice cover and/or an increase in Southern Ocean upwelling. If the general picture emerging from reconstructions is realistic, then the model-data mismatch in mid and high Southern Hemisphere latitudes implies that none of the models is able to resolve the correct balance of these feedbacks, or, alternatively, that interglacial Southern

* Corresponding author.
  E-mail address: pbakker@coas.oregonstate.edu (P. Bakker).
[1] Now at Swedish Meteorological and Hydrological Institute (SMHI), Norrköping, Sweden.

Hemisphere temperature trends are driven by mechanisms which are not included in the transient simulations, such as changes in the Antarctic ice sheet or meltwater-induced changes in the overturning circulation.

1. Introduction

It has long been recognised that changes in the astronomical configuration of the Earth's orbit are a primary driver of long-term climate variations (Milankovitch, 1941). Past changes in the latitudinal and seasonal distribution of incoming top-of-the-atmosphere solar radiation (referred to as insolation in this manuscript) can be accurately calculated (Berger, 1978; Berger and Loutre, 1991; Laskar et al., 2004). The response of the climate system to this astronomical forcing includes a diversity of feedbacks involving the atmosphere, ocean, sea ice, vegetation and land ice (Braconnot et al., 2012; PALAEOSENS Project Members, 2012). Palaeoclimate information can be used to assess the realism of the representation of these feedbacks within numerical climate models. Systematic model-data comparisons performed within the Paleoclimate Modelling Intercomparison Project (PMIP) have focused on time-slice experiments such as those performed by Braconnot et al. (2007) for the middle of the Present Interglacial period (PIG-period) and by Lunt et al. (2013) for the thermal maximum of the Last Interglacial period (LIG-period; note that throughout the text PIG-period and LIG-period refer loosely to the two interglacial periods, while PIG and LIG will be used to indicate the specific target intervals defined in Section 2.1). During the last decade, progress has been made in the documentation of past climate variability based on time series from geological archives (e.g. deep-sea sediments, ice cores, lake sediments) resulting in a large number of proxy-based temperature reconstructions for the PIG-period (e.g. Wanner et al., 2008; Lohmann et al., 2013; Marcott et al., 2013) and, to a lesser extent, for the LIG-period (Andersen et al., 2004; CAPE Last Interglacial Project Members, 2006; Turney and Jones, 2010; McKay et al., 2011), with improved age models (e.g. Waelbroeck et al., 2008; Masson-Delmotte et al., 2011b). In parallel, increasing computational capacity, as well as the development of more computationally efficient climate models, has made it feasible to perform multi-millennial climate simulations (Bakker et al., 2013; Langebroek and Nisancioglu, 2013; Lohmann et al., 2013). These lines of progress now allow an investigation of PIG-period and LIG-period multi-millennial temperature trends, e.g. multi-millennial linear temperature changes, based on multiple reconstructions and simulations. The assessment of the ability of climate models to reproduce climate trends during periods warmer than today is strongly motivated by the context of projected global warming. Indeed, while there is no direct analogy between the physics of greenhouse gas versus astronomical forcing, the LIG-period is characterised by Northern Hemisphere (NH) continental summer temperatures that are similar to those expected for the coming centuries (Masson-Delmotte et al., 2010b).

The PIG-period (~12 ka until the present-day; throughout this manuscript we will use [ka] to indicate kiloyears before 1950) and the LIG-period (~130–115 ka) are both warm interglacial periods with distinct $\delta^{18}O$ values in both ice-core and deep-sea-sediment records. Extensive research has resulted in a large number of proxy-based temperature reconstructions for the PIG-period (e.g. Wanner et al., 2008; Lohmann et al., 2013; Marcott et al., 2013) and (to a lesser extent) for the LIG-period (Andersen et al., 2004; CAPE Last Interglacial Project Members, 2006; Turney and Jones, 2010; McKay et al., 2011). For most mid-to-high latitude NH regions,

the temperature evolution of the PIG-period is characterised by a gradual 1 °C decrease of the summer temperature from the early part of the interglacial to the pre-industrial situation. This multi-millennial temperature trend has been attributed to insolation changes (Wanner et al., 2008; Renssen et al., 2009). However, there are significant spatial differences in the magnitude and timing of the early PIG-period temperature maximum, and therefore in the PIG-period temperature trends, which are related for instance to the cooling effect of remnants of NH glacial ice sheets (Renssen et al., 2009). Lohmann et al. (2013) have recently shown that climate models underestimate reconstructed sea surface temperature (SST) changes over part of the PIG-period and that overall the model-data disagreement becomes smaller if seasonal biases in the proxy-based temperature trends are taken into account.

Climate reconstructions from the LIG-period show that maximum temperatures were roughly 2–5 °C higher than at present in, respectively, the mid- and high-latitudes of the NH (CAPE Last Interglacial Project Members, 2006; Turney and Jones, 2010; McKay et al., 2011; Sánchez-Goñi et al., 2012) during the early part of the LIG-period (>~126 ka; Sánchez-Goñi et al., 2012; Shackleton et al., 2003). In Antarctica, LIG-period peak warmth (temperature anomalies of at least 4 °C; Sime et al., 2008; Masson-Delmotte et al., 2011b), was shown to occur earlier than at NH high latitudes (Masson-Delmotte et al., 2010a; Govin et al., 2012). However, the number of climate reconstructions available for the LIG-period is much smaller than for the PIG-period. Moreover, mainly because the LIG-period lies outside the time span covered by ^{14}C dating techniques or ice-core layer counting, climate reconstructions are hampered by important issues related to assigning absolute ages and, as a consequence, to aligning different time series.

In addition to proxy-based reconstructions, transient climate-model experiments are helpful for analysing the PIG-period and LIG-period climates. If forced by the best estimate of millennial-scale astronomical and greenhouse gas (GHG) forcing scenarios at hand, simulations allow us to i) provide a global picture of the surface temperature evolution and ii) to investigate the role of external forcings and climate feedbacks in shaping the seasonal evolution of temperature. Earlier model-data comparisons focused on equilibrium simulations (Lunt et al., 2013). Beyond this approach, the transient nature of the simulations presented here enables us to i) describe the dynamical temperature response to the evolution of the astronomical forcing in the PIG-period and the LIG-period and ii) to take into account feedbacks from parts of the climate system which have a long (>1 ka) response time such as the deep ocean. A model inter-comparison of transient simulations covering the later part of the PIG-period, 6 ka to present, has been described in an earlier review study by Wanner et al. (2008). Their main findings are a decrease in summer temperatures at mid and high NH latitudes while winter temperatures decrease north of 60°N and increase at the mid latitudes of the NH. Results from the equatorial region and the Southern Hemisphere (SH) tend to differ between the different simulations. In a more recent model inter-comparison of transient PIG-period simulations, Varma et al. (2012) found a consistent cooling trend over Antarctica and the adjacent ocean between 7 and 0.25 ka. Model inter-comparison

studies for LIG-period simulations have been undertaken within the framework of the PMIP3 project. The time slice experiments reviewed by Lunt et al. (2013) for the early part of the LIG-period, between 130 and 125 ka, show that annual mean changes compared to present-day only demonstrate a robust warming in the Arctic region and a cooling in the African and Indian monsoon regions. The seasonal signal tends to be more robust and shows a summer warming over the mid-to-high latitudes of the NH and an overall cooling of DJF with the exception of the Arctic where a warming is simulated in winter. Lunt et al. (2013) have shown that LIG-period equilibrium simulations are in poor agreement with reconstructed LIG-period annual mean and seasonal temperature changes. A number of transient LIG-period simulations, all of them included in this manuscript, have been inter-compared by Bakker et al. (2013). When the transiently simulated temperatures for the early part of the LIG-period are compared with the time slice experiments many similarities are found. However, Bakker et al. (2013) stress that the temperature evolution in specific regions is strongly altered by highly model-dependent feedbacks within the climate system related to the Meridional Overturning Circulation (MOC), sea ice, remnants of glacial continental ice sheets and monsoon dynamics, a conclusion which is in line with that found for the Mid-Holocene by Otto-Bliesner et al. (2006). The simulated transient LIG temperatures have, however, not yet been compared to reconstructed temperatures or to simulated transient PIG-period temperatures.

In this study we therefore combine PIG-period and LIG-period transient simulations from 9 different climate models including fast coupled ocean-atmosphere general circulation models (GCMs) and intermediate complexity models (EMICs). Including two different interglacial periods in the inter-comparison enables us to describe patterns in interglacial temperature trends that are likely valid for interglacial periods in general, because climate change features specific to either the PIG or the LIG can be isolated. Here one can think, for instance, of climatic changes caused by changes in the global ocean circulation. Moreover, the comparison of PIG and LIG allows us to address the question whether interglacial climate reacts, to a first order, linear to the orbital forcing. The fact that the PIG-period and LIG-period climates are simulated with the same models offers the opportunity to analyse the impact of the forcings within each model. Including results from various climate models that differ from one another in a number of ways (e.g. model sensitivity, setup and resolution, the degree to which different processes are parameterised and the extent of coupling between the various subcomponents of the climate system), yields robust multi-model results that are largely model independent. These multi-model transient temperature simulations are combined with a new compilation of reconstructed temperature time-series for the PIG-period and the LIG-period. Because of the highly complex nature of such a large multi-model-data comparison, we limit the analysis to the first order temperature changes, e.g. multi-millennial linear temperature trends. Furthermore, our focus will be on specific sub-intervals of the PIG- and LIG-periods as defined in Section 2.1. We will address the following questions:

1) Are there temperature trends that are common to reconstructions and simulations?
2) Are the magnitudes as well as the spatial patterns of the temperature trends different during the PIG and LIG?
3) What are the caveats linked to proxy record interpretation and/ or missing feedbacks in the simulations?
4) Are the PIG and LIG temperature trends linearly related to the astronomical forcing? If not, can we identify the non-linear processes operating on multi-millennial time scales?

2. Material and methods

2.1. Defining Present and Last Interglacial target intervals

To consistently compare both reconstructed and simulated PIG-period and LIG-period temperature trends we need to define target intervals. Our main criterion in defining these intervals is that the rate of change of the underlying astronomical forcing should be comparable between the two interglacial intervals. To meet this criterion, an alignment of the PIG-period and the LIG-period is needed. For this purpose, we identified the timing of the maximum change in the climatic precession (defined as the eccentricity times the sine of the longitude of the perihelion; Fig. 1) in the PIG-period and the LIG-period, at 6.0 ka and 121.0 ka respectively. This approach is taken because climatic precession appears to be of large importance for PIG-period and LIG-period seasonal insolation changes (Fig. 1). In order to have comparable astronomical forcing trends in the two intervals, a further restriction is that the sign of the trend in the climatic precession parameter does not change (i.e. only negative trends in climatic precession parameter), between 12.3–1 ka and 127.2–116.2 ka for the PIG-period and LIG-period, respectively. Finally, combining the described interval limits and the alignment with constraints imposed by the intervals of the performed simulations (8–0 ka for the PIG-period and 130–115 ka for the LIG-period) and the requirement that for consistency both intervals should have the same length. This provides the following definition of the specific PIG and the LIG intervals: 8–1.2 ka and 123–116.2 ka, hereafter referred to as simply PIG and LIG respectively (grey band in Fig. 1).

The defined intervals do not cover the whole interglacial periods and particularly not the warmest, earliest part of the Last Interglacial. While they are selected as two intervals with similar signs of climatic precession changes, they differ in (i) the magnitude of the climatic precession and seasonal insolation changes; and (ii) the mean levels of eccentricity (higher for the LIG) and obliquity (higher for the PIG; Fig. 1). Our intervals and alignment are therefore purely constructed for an analysis of the climate feedbacks with respect to a given climatic precession trend, and cannot be used for other purposes such as investigating the ending of interglacial periods (e.g. Ruddiman et al., 2005).

2.2. Climatic forcings of the PIG and LIG intervals

The evolution of PIG GHG concentrations and the corresponding radiative forcing is characterised by a small rising trend, while for the LIG stable concentrations have been reconstructed (Fig. 1). The differences between the GHG radiative forcing of the pre-industrial period, the PIG and the LIG are small, less than ~0.5 Wm^{-2}. By contrast, both the PIG and LIG are characterised by substantial changes in the spatial and temporal distribution of insolation. Because of the decrease in obliquity and the increase in climatic precession, PIG and LIG NH summer (JJA) insolation decreases while winter (DJF) insolation increases and as a result there is a small decrease in annual insolation north of ~43°N (Fig. 2). In contrast to the NH, SH summer (DJF) insolation is increasing and winter (JJA) insolation decreasing. The evolution of annual mean insolation shows decreasing values at latitudes larger than ~43° in both hemispheres (Fig. 2). The evolution of insolation during the PIG and LIG intervals shows many similarities. However, because of larger eccentricity values during the LIG, a different phasing of obliquity and climatic precession, and larger changes in climatic precession during the LIG compared to the PIG (Fig. 1), the magnitude of the annual, seasonal and latitudinal insolation changes is larger during the LIG than in the PIG (Fig. 2). The different magnitudes of the insolation trends motivate a focus on
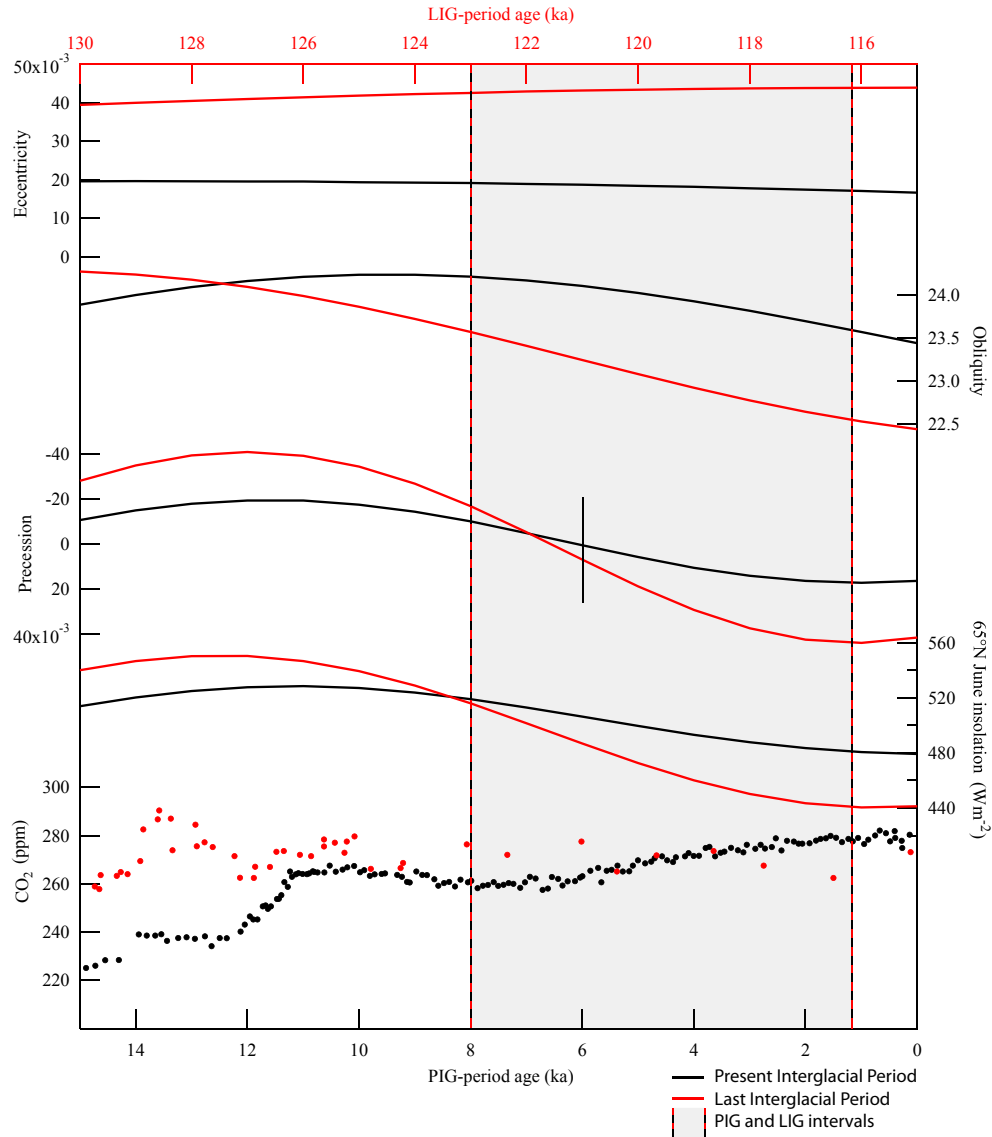
Fig. 1. Climate forcings during the PIG and the LIG. Climate forcings during the PIG-period (black; bottom age scale) and LIG-period (red; top age scale). From top to bottom: Eccentricity, obliquity (°), climatic precession (defined as the eccentricity times the sine of the longitude of the perihelion; note reversed vertical axis), June insolation at 65°N (Laskar et al., 2004) and ice-core based reconstructed CO_2 concentrations (Luthi et al., 2008; in accordance with the PMIP3 protocol). The climate simulations run from 8 to 0 ka and 130 to 115 ka for the PIG-period and LIG-period respectively (for the exceptions see Table 1). The alignment of the two intervals is based on the maximum rate of change in the precession cycle at 6 ka and 121 ka (indicated by the small vertical black line). The grey area indicates the PIG (8—1.2 ka) and LIG (123—116.2 ka) intervals used throughout the manuscript to calculate interglacial trends. (For interpretation of the references to colour in this figure legend, the reader is referred to the web version of this article.)

the dynamical aspect of the climate system, a comparison of reconstructed and simulated, PIG and LIG temperature trends.

2.3. Reconstructing the temperature evolution

In this model-data comparison, we use the so-called PIG2LIG-4FUTURE database temperature compilation that resulted from a compilation effort of the research community within the Past4Future project (European Union's Seventh Framework Programme; FP7/2007—2013; El Ouahabi et al., in prep). This database includes temperature estimates from alkenone records measured in marine sediment cores retrieved from the Atlantic, Southern, Mediterranean, Indian and Pacific basins and from stable water-isotope ratios measured in ice cores from Greenland and Antarctica. The aim of preparing this compilation was to provide a regional synthesis of anomalies with sufficient time resolution and sufficient spatial

coverage to estimate PIG and LIG multi-millennial temperature trends at a global scale. For the purpose of simplicity, only two proxy types (alkenones and stable water isotopes) are considered here. We are aware that each proxy type is associated with systematic artefacts, and that temperature estimates may differ from those inferred from other proxies. A recent example of a comparison between alkenone and Mg/Ca-derived PIG SSTs can be found in Lohmann et al. (2013).

Alkenones are lipidic organic compounds synthesized by the coccolithophora flora (Brassell et al., 1986; Thierstein and Young, 2004). Their unsaturation degree increases immediately if the temperature changes, which is a characteristic, physiological response of membrane lipids or metabolic storage molecules (Prahl and Wakeham, 1987; Prahl et al., 1988; Epstein et al., 2001). Commonly, integrated sedimentation patterns for alkenones measured in sediment trap time-series and surface marine
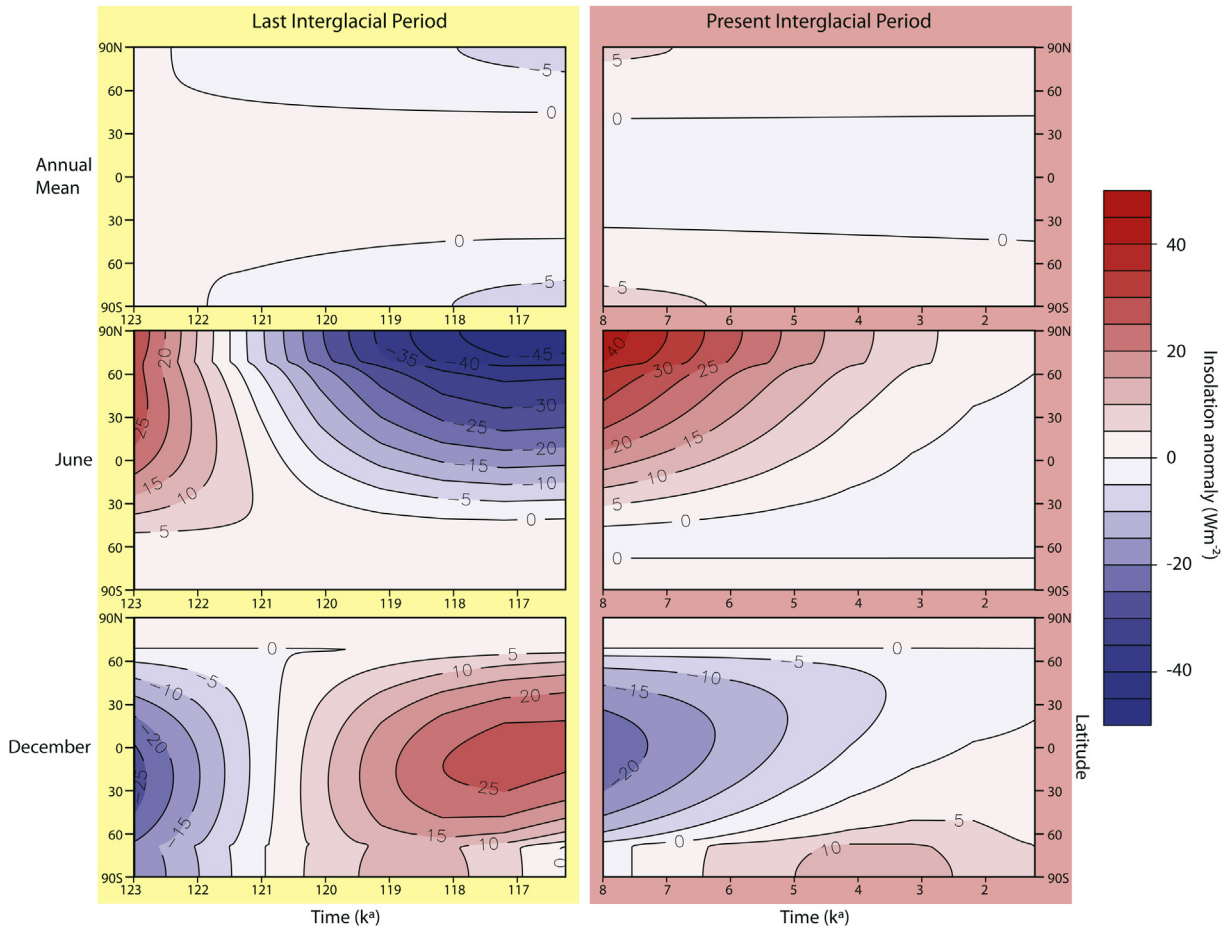
Fig. 2. Latitudinal differences in the evolution of PIG and LIG insolation anomalies. For the PIG (right) and the LIG (left) the evolution of the latitudinal insolation anomalies (Wm^{-2}; Laskar et al., 2004) compared to pre-industrial times are shown for annual mean (top), June (middle) and December (bottom). In line with the simulations, the monthly mean insolation anomalies have been calculated using a fixed-day calendar.

sediments show a good match with annual mean SSTs (Rosell-Melé and Prahl, 2013). Local processes, such as upwelling along ocean-basin margins or surface transport (e.g. Sicre et al., 2005; Rühlemann and Butzin, 2006), are a potential source of bias in some individual records. However, regional or global signals likely overwhelm these local biases in a multi-centennial and multi-record synthesis.

In this model-data comparison we included from the PIG2LIG-4FUTURE database a total of 49 alkenone-based temperature records for the PIG interval and 30 that cover the LIG interval. Of the 30 LIG alkenone records, 21 cover both PIG and LIG while only a single record covers only the LIG. For a small number of sites that are located within a 1°-radius, an average temperatures where calculated. References to the original papers that describe the individual alkenone records can be found in Appendix Table A.1.

Reproducibility tests show that analytical uncertainty in the alkenone unsaturation index determination is always lower than 0.0165 (ca 0.5 °C). By using a proper sediment calibration (i.e. using cultures, water column particulate organic matter or core-top sediments), it is possible to estimate temperatures from this index. Some calibrations could be considered as global (e.g. Müller et al., 1998; Conte et al., 2006); others are useful for specific restricted regions (e.g. Rosell-Melé et al., 1995 for the Arctic; Sonzogni et al., 1997 for the Indian Ocean; Pelejero and Grimalt, 1997 for the South China Sea). Considering uncertainties, the SSTs reconstructed from alkenones depend only slightly on the calibration that is used and they agree remarkably well with the

culture experiments that have been performed to verify the coccolithophore response to temperatures (Prahl and Wakeham, 1987; Prahl et al., 1988). To facilitate the model-data comparison, we sum up the analytical uncertainty of 0.5 °C with an uncertainty of 1.2 °C based on the different calibration techniques described above. Core-top estimations in the alkenone records were extracted by calculating the average of the period around the last two millennia. Instrumental annual mean SSTs (taken from Locarnini et al., 2010, World Ocean Atlas, 2009; 2 × 2 grid cells) and core-top, alkenone-based temperatures are in agreement within calibration uncertainties in the subtropics and mid latitudes.

For all alkenone records presented here, the original chronologies have been used. An unquantified source of uncertainty therefore arises from the uncertainty on the dating of deep sea sediment core records (El Ouahabi et al., in prep). This dating uncertainty for the LIG-period ranges from 2 ky at best to 6 ky, in case of incorrect orbital targets (Bazin et al., 2012). The average sampling frequency of the alkenone records is around 1 sample every 0.6 ky for the PIG and every 1.7 ky for the LIG with the time resolution varying from multi-decadal to millennial in both periods. The number of samples used to calculate the linear temperature trends are listed in Appendix Table A.1.

The alkenone-based multi-millennial temperature trends used in this manuscript are based on a linear least squares regression (Appendix Table A.1). The same procedure is applied to the ice-core-based temperature trends and the simulated temperature trends. We acknowledge that a linear model is not a perfect

description of the interglacial climate response, as is clear from some of the R-squared values listed in the Appendix Table A.1, but it does characterise the first order response of the changes in temperature on multi-millennial time scales (Lohmann et al., 2013). Furthermore, the number of data points available to perform the calculations is sometimes limited (Appendix Table A.1). Note that, despite the applied local linear approximation, differences in the insolation trends between the PIG and the LIG and between different regions can still result in an overall nonlinear response between insolation trends and temperature trends.

Regarding alkenone records at mid- and high-latitudes (>30°N and >30°S), the trends of the SST progression during the LIG (average -0.35 °C ky^{-1}, $n = 14$) are generally steeper than during the PIG (average -0.22 °C ky^{-1}, $n = 28$), and higher for the NH (average -0.32 °C ky^{-1}, $n = 32$) than for the SH (average -0.22 °C ky^{-1}, $n = 10$). At low latitudes (between 30°N and 30°S) trends during the LIG appear to be three times larger than during the PIG and of the opposite sign, i.e. slight cooling for the LIG (-0.13 °C ky^{-1}, $n = 17$) versus no trend or warming for the PIG ($+0.04$ °C ky^{-1}, $n = 19$). The overall 1.7 °C error in the temperature reconstruction leads to an uncertainty estimate of 0.5 °C ky^{-1} in the alkenone-based temperature trends over the 6.8 ky intervals (Appendix Table A.1). Note, that the alkenone-based temperature trends including the 0.5 °C ky^{-1} uncertainty estimate, are often not significantly different from zero. The compilation of alkenone records and the resulting temperature trends used in this study are to a large extent similar to the ones published by Lohmann et al. (2013) although a direct comparison of the temperature trends is hampered by the fact that the definition of the PIG intervals are different.

Stable water-isotope ratios from ice cores are related to past changes in precipitation-weighted condensation temperature, due to the impact of atmospheric temperature on condensation and water vapour distillation (Jouzel et al., 2003; Masson-Delmotte et al., 2006; Jouzel and Masson-Delmotte, 2010). Quantitative temperature reconstructions however remain limited by the fact that the stable water isotope temperature relationship may vary through time, due to changes in the seasonality of precipitation (Sime and Wolff, 2011; Laepple et al., 2011), changes in moisture origin (Stenni et al., 2010) and trajectories, or changes in ice-sheet topography (Bradley et al., 2012). From deuterium-excess records, changes in moisture origin appear to have limited impacts for the time periods investigated here (Masson-Delmotte et al., 2011b; Uemura et al., 2012).

By combining information from several Greenland ice cores (Agassiz, Renland, DYE3, GRIP, NGRIP and Camp Century) a mean PIG elevation-corrected temperature trend of -0.34 °C ky^{-1} is retrieved. Data from the NEEM ice core (the only ice core on Greenland that spans the whole of the LIG) yield a LIG elevation-corrected temperature trend of -1.32 °C ky^{-1}. The chronologies of the LIG Greenland ice core records used in this study are synchronised to Antarctic ice cores using the EDC3 age scale (Parrenin et al., 2007; Masson-Delmotte et al., 2011b) and are re-sampled to a common 100 yr time step. For a detailed description of the resolution and chronology of the Greenland ice cores we refer to Vinther et al. (2009) and NEEM community members (2013). Ice-core-based PIG and LIG temperature trend reconstructions for Antarctica (here without elevation correction) are based on the cores that have been synchronised on the EDC3 age scale, namely TALDICE, EDC, EDML, Dome F and Vostok with resulting trends of 0.20, 0.08, 0.0, -0.18 and -0.08 °C ky^{-1} for the PIG and -0.25, -0.37, -0.42, -0.51 and -0.32 °C ky^{-1} for the LIG, respectively. In the EDC3 age scale, the uncertainty associated with the duration of the LIG-period, which in turn impacts the resulting LIG interval, is estimated to be 20% (~3 ky; Parrenin et al., 2007). We note that a revised Antarctic ice core chronology (AICC2012) shows

very similar durations of the PIG-period (within 2.5%) and the LIG-period (within 5%) with EDC3 (Bazin et al., 2012). The resolution of the Antarctic ice cores is 10–20 yrs for the PIG and 25–115 yrs for the LIG (Masson-Delmotte et al., 2011b).

Determining the level of uncertainty for the different ice-core-based temperature reconstructions is very difficult. We assume here a simplistic minimum absolute uncertainty of 1 °C for the ice-core-based temperature reconstruction and translate this into a 0.29 °C ky^{-1} uncertainty for the temperature trends over the 6.8 ky intervals. This does not account for biases due for instance to changes in the seasonality of precipitation, which cannot be quantified from ice core data.

2.4. Simulating the temperature evolution

We used eight multi-millennial transient simulations for the PIG and nine for the LIG. The climate models used for these simulations vary widely in their degree of complexity, the incorporated components of the climate system and the applied transient climate forcings. In this manuscript only the most important differences between the simulations are listed (see also Table 1 and the references therein).

This model inter-comparison includes EMICs (Bern3D, CLIMBER2 and LOVECLIM) and GCMs (CCSM3, CSIRO, COSMOS, FAMOUS, KCM and MPI-UW). Supported by members of the Past4Future project (http://www.past4future.eu/), multi-millennial transient simulations for the PIG-period and LIG-period have been formalised within the PMIP3 protocol (http://pmip3.lsce.ipsl.fr/). Within this protocol, the time frame for respectively the PIG-period

Table 1
Specifics of the climate simulations. Summary of the main features of the different models in this inter-comparison and the forcing scenarios applied. The acronyms in the table are: EMIC = Earth system Model of Intermediate Complexity; GCM = General Circulation Model; OC = Ocean; AT = Atmosphere; VE = Vegetation; SI = Sea Ice; IS = Ice Sheet; CA = Carbon Cycle; Norm = Normal (non accelerated); Acc = Accelerated; GHG = Greenhouse-gas forcing; FWF = Freshwater Forcing. When no transient GHG forcing is applied the values are fixed at pre-industrial levels (KCM and the PIG CCSM3 simulation) or at average LIG values (LIG CCSM3 simulation). The grey shading for COSMOS is used to indicate that for the PIG (LIG) simulation a vegetation component is (is not) included and that the GHG concentrations in the PIG (LIG) simulation are fixed (transient). The GHG concentrations in the MPI-UW simulation are calculated interactively and therefore differ from the other simulations. Furthermore, the MPI-UW simulations have been performed in a periodically synchronous mode. For more detailed information about the climate models and the forcing scenarios see Bakker et al. (2013; only LIG simulations performed with Bern3D, CCSM3, CLIMBER2, FAMOUS, KCM, LOVECLIM and MPI-UW) and the following publications: Bern3D (Edwards and Marsh, 2005; Müller et al., 2006; Ritz et al., 2011a, 2011b); CCSM3 (Collins et al., 2006; Varma et al., 2012); CLIMBER2 (Petoukhov et al., 2000); COSMOS (Marsland et al., 2003; Roeckner et al., 2003); CSIRO (version CSIRO-Mk3L-1.2; Phipps et al., 2011, 2012); FAMOUS (Gordon et al., 2000; Jones et al., 2005; Smith, 2012; Smith and Gregory, 2012); KCM (Park et al., 2009); LOVECLIM (Goosse et al., 2010); MPI-UW (Gröger et al., 2007; Mikolajewicz et al., 2007).

	Model type		Climate components						Transient climate forcings				
	EMIC	GCM	OC	AT	VE	SI	IS	CA	Orbital		GHG	IS	FWF
Model name									Norm	Acc			
Bern3D													
CCSM3													
CLIMBER2													
COSMOS													
CSIRO													
FAMOUS													
KCM													
LOVECLIM													
MPI-UW													
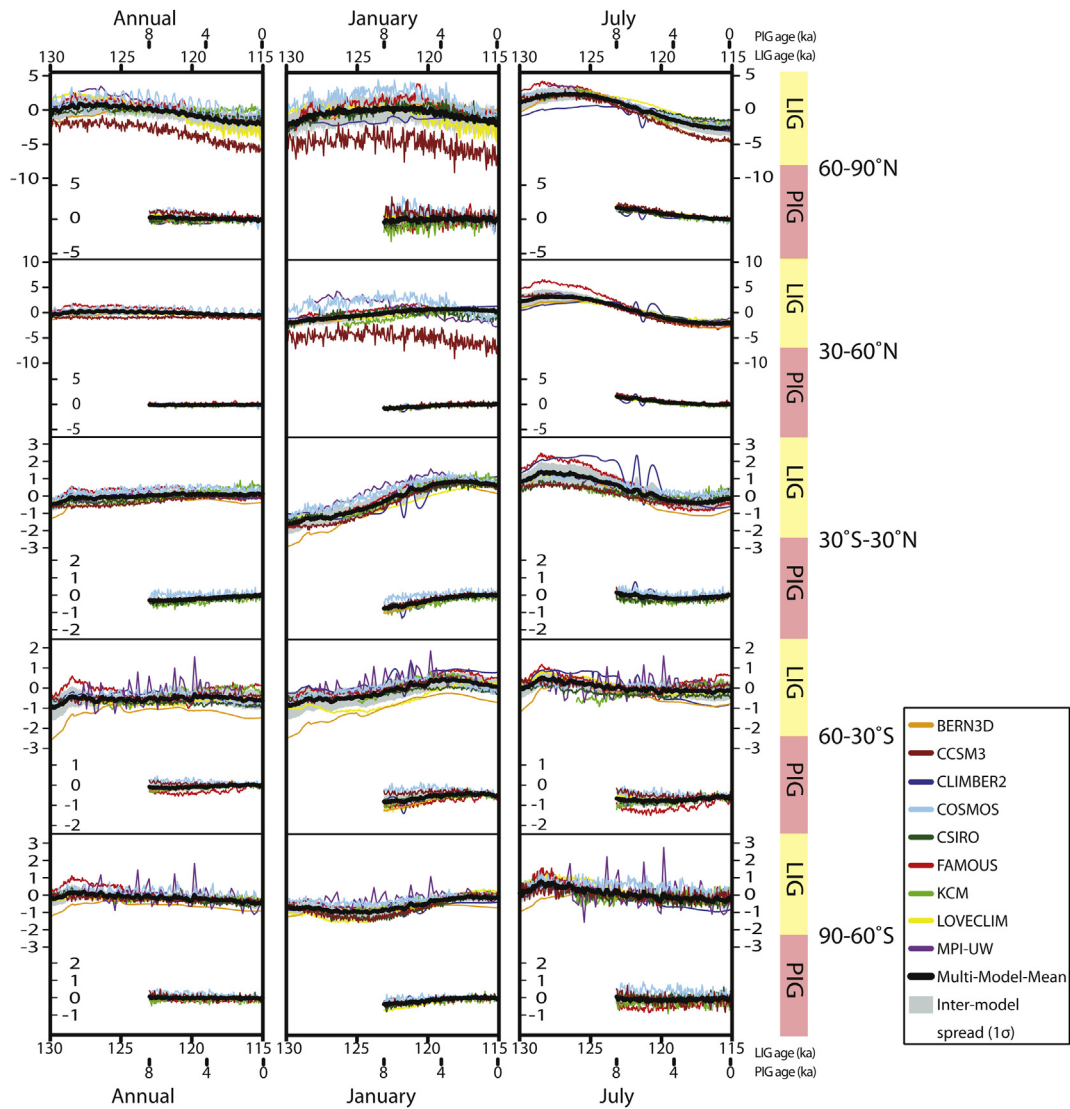
Fig. 3. Simulated PIG and LIG temperature evolution. Simulated temperature evolution covering a large part of the PIG-period (8–0 ka) and LIG-period (130–115 ka). Temperatures anomalies relative to a control period (1850–1950). The five rows give averages over five different latitude bands (after Bakker et al., 2013) and the three columns give the temperature evolution for (from right to left) the annual mean, January and July temperatures. Every panel displays the temperature evolution for the LIG-period (top) and PIG-period (bottom). The different colours correspond to the individual model simulations. The bold black curve indicates the Multi-Model-Mean and the grey area indicates the spread (1σ) around this mean. Note that within each latitude band the scaling of the y-axis is consistent, but that it differs between the bands. (For interpretation of the references to colour in this figure legend, the reader is referred to the web version of this article.)

and the LIG-period is set to 8–0 ka and 130–115 ka and the values of the astronomical and GHG forcings are prescribed. Furthermore, the protocol describes the spin-up procedure (a 2 ky period with respectively 10–8 ka or 132–130 ka transient astronomical and GHG forcings) and specifies that sea-level height, vegetation and ice-sheet extent and thickness be fixed to present-day values. Several of the simulations have been performed in accelerated mode with a 10-fold increase in the rate of change of the astronomical forcing (CCSM3, COSMOS, CSIRO and KCM). For the multi-millennial time scales under consideration in this manuscript, the impact of the applied acceleration technique can be regarded as negligible on the atmosphere and ocean mixed layer (Lorenz and Lohmann, 2004), and its potential impact on the deep-ocean circulation is discussed in Section 3.4.3. Some simulations differ from the PMIP3 protocol in either the time span or the forcings. In the Bern3D simulations, remnants of glacial ice and a corresponding meltwater flux are prescribed. Other simulations deviating from the PMIP3 protocol are the CCSM3 simulations that are performed

with fixed GHG concentrations at either pre-industrial (PI) levels for the PIG-period or average LIG-period levels for the LIG-period. The CLIMBER2 simulations include dynamical vegetation computations, as does the PIG-period simulation performed with COSMOS which also has fixed GHG concentrations. The KCM LIG-period simulation only runs from 126 ka to 115 ka. The MPI-UW simulation runs from 128 ka to 115 ka and includes a dynamical terrestrial and marine carbon-cycle model with a prognostic GHG forcing. As a result, in the latter simulation the GHG forcing is rather different from the reconstructed GHG concentrations prescribed in the PMIP3 protocol. This manuscript does not include a MPI-UW PIG simulation.

In order to standardise all the different simulations we regridded all outputs onto a common 1° × 1° grid and calculated 50-year averages for every month. The temperatures are presented as anomalies compared to the last 100 yrs of the PIG-period simulation (i.e. 1850–1950 AD). Since no PIG simulation is available for MPI-UW, in this case an average was taken over the last 100 yrs of a
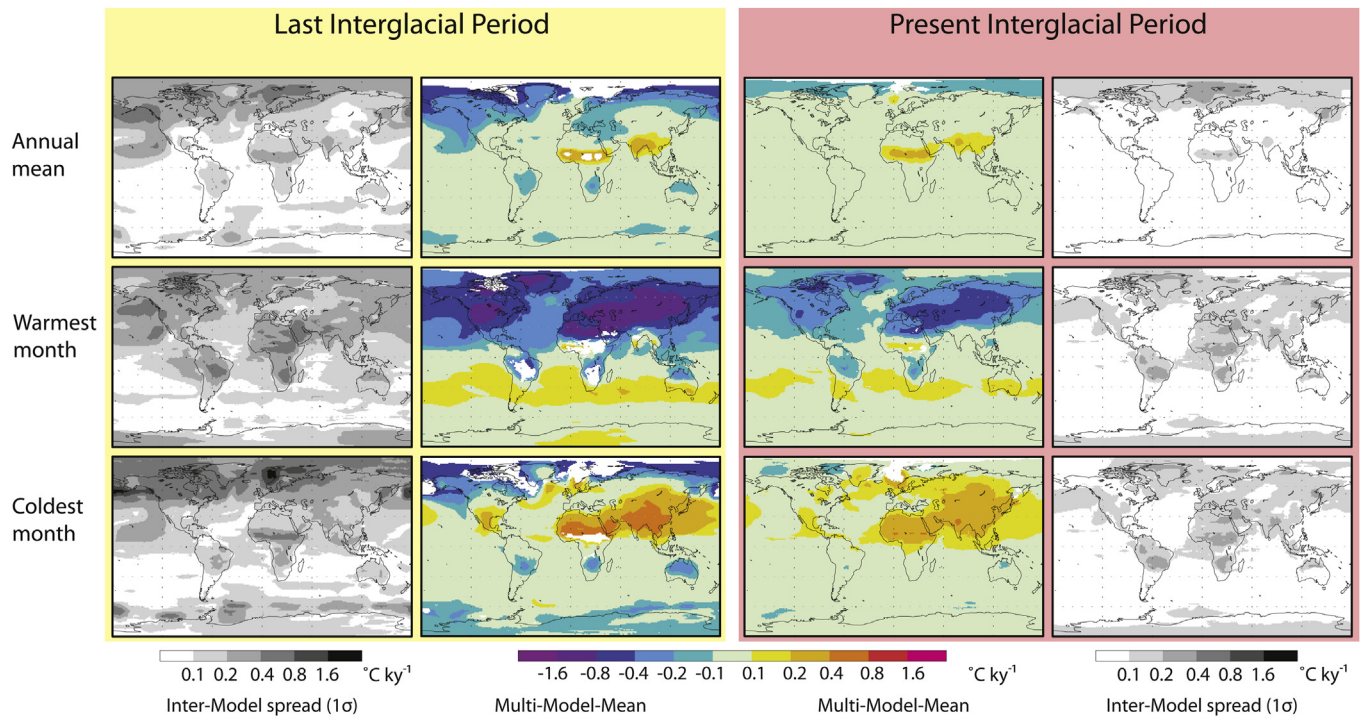
Fig. 4. Simulated PIG and LIG temperature trends. Overview of the Multi-Model-Mean (MMM) multi-millennial temperature trends and the spread around this mean for the PIG (right) and the LIG (left; see Results section for a detailed description of the performed calculations). The rows indicate (from top to bottom): annual temperatures, warmest-month temperatures and coldest-month temperatures. The two middle columns give the MMM multi-millennial temperature trends ($°C\ ky^{-1}$). Note that the white shading in the MMM plots indicates that the different simulations do not give a consistent signal. The two outer columns give the inter-model spread (1σ) around the MMM.

pre-industrial equilibrium simulation. In this manuscript, simulated temperatures refer to near-surface-air temperatures. This affects the model-data comparison, especially when alkenone-based temperature reconstructions are concerned, because these are calibrated towards SSTs. However, on multi-millennial time scales, trends in SSTs and the temperature of the overlying atmospheric layer can be assumed to be closely linked (Jones et al., 1999). Exceptions are the sea-ice covered areas, but since there are almost no alkenone data from such regions in our synthesis, this will not have an important impact on our model-data comparison. In the calculation of the warmest- and coldest-month temperatures presented in this manuscript, we used present-day calendar months. This implies that the warmest or coldest month is not necessarily the warmest or coldest 30-day period of that specific year. Furthermore, there are large regional differences in the occurrence of the warmest month throughout the year, differences that are further elaborated in Section 3.4. Finally, in all the simulations presented in this manuscript, present-day calendar months are used. This should be kept in mind when comparing simulated monthly temperatures with proxy-reconstructions since it can have a substantial effect on calculated monthly temperatures for the late summer and autumn seasons (Joussaume and Braconnot, 1997).

Most of the simulated PIG-period and LIG-period temperature time-series investigated in this manuscript have previously been published elsewhere. We therefore only present the simulated PIG-period and LIG-period temperature time-series in Fig. 3 and refer to Bakker et al. (2013) for a more thorough description.

3. Results and discussion

3.1. Simulated temperature trends

To investigate the temporal variations of simulated interglacial temperatures, we calculate linear temperature trends over the defined PIG and LIG intervals. To make the comparison of model results with findings from proxy-based reconstructions feasible, we aim to construct multi-model mean (MMM) temperature trends. As for the reconstructed temperature trends, the simulated temperature trends are linear least squares fits to the 50-year average temperature data. To ensure this MMM captures all features that are common to the majority of the included climate models we take the following steps: First we test if a trend from an individual model is consistent with the other models by comparing it to a pre-determined threshold value. This threshold is chosen such that it represents the amplitude of the simulated internal climate variability in terms of temperature trends. Since this variability is expected to vary mostly with latitude, a latitudinal-dependent threshold is constructed by taking a longitudinal root-mean-square-average over the inter-model spread (grid point standard deviation among the models; 1σ) for each $1°$ latitude band (Fig. 4). Second, the local MMM temperature trend at each $1 \times 1°$ grid point is only considered to be consistent if at least 70% of the temperature trends simulated by the individual climate models at that grid point are within the MMM plus or minus the threshold value. Notwithstanding that the determination of the consistency of the MMM temperature trends is somewhat arbitrary, additional sensitivity experiments have revealed that the general picture provided by the MMM is insensitive to the precise definition of the threshold value (1, 5 or $10°$ latitude bands) or cut-off value (60%, 70% or 80%).

Overall the simulated temperatures for different seasons show larger multi-millennial MMM trends for the LIG than for the PIG (Fig. 4) and fairly good agreement amongst the models (inter-model spread in Fig. 4 is generally small). Exceptions are the temperature trend patterns in regions such as the Arctic, the Sahel and Indian monsoon regions, and most of the SH. Generally PIG and LIG annual mean temperature trends (AMTTs) are small and comparable (PIG ~0; LIG ~−0.1 $°C\ ky^{-1}$ in global mean) but over the Arctic the LIG AMTTs are much larger than the PIG trends (~−0.2 to
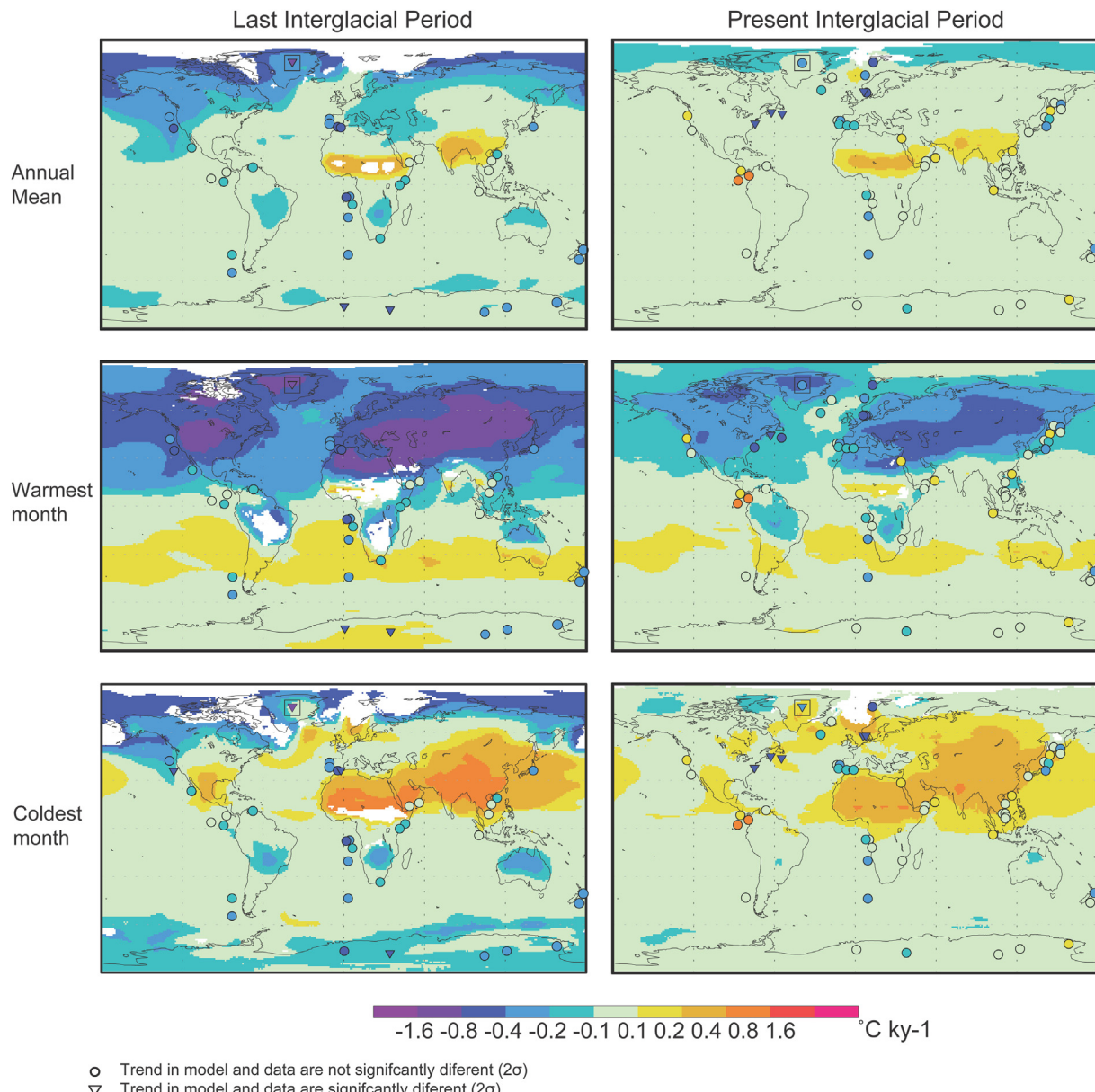
Fig. 5. Geographical comparison of simulated and reconstructed PIG and LIG temperature trends. PIG (right) and LIG (left) simulated Multi-Model-Mean (MMM) multi-millennial temperature trends (°C ky^{-1}; shaded; see results section for a description of the construction of the MMM temperature trends) and the proxy-based multi-millennial temperature trends (symbols). The plots show (from top to bottom) simulated annual mean temperature trends (AMTT), warmest-month temperature trends (WMTT) and coldest-month temperature trends (CMTT). The white shading indicates that the different simulations do not give a consistent signal. All panels show both alkenone-based temperature trend reconstructions and the δ^{18}O-based temperature trend reconstructions from ice cores. The box around the Greenland data indicates that the ice-core-based temperature trend is based on a number of Greenland ice cores. The model-data comparison is performed by calculating *t*-test statistics for the reconstructed temperature trend and the simulated MMM trend. The simulated temperature trends corresponding to the proxy-based temperature trend reconstructions are averaged over an area of 3° by 3° centred on the location of the proxy site. If model and data are not significantly different (at 5% probability) this is indicated by a circle shaped symbol, if they are significantly different a triangle shaped symbol is used. In the PIG coldest-month panel the alkenone record from 67°N and 8°E is masked out because the models do not agree amongst each other and thus a model-data comparison could not be performed. Note that the seemingly good correspondence derived from the statistical analysis is in part due to the large uncertainties for both model and data.

~−0.6 °C ky^{-1} for PIG and LIG respectively). During the warmest month, the LIG trend is largest over the NH continents (PIG ~−0.3; LIG ~−0.6 °C ky^{-1}) and the North Atlantic (PIG ~−0.1; LIG ~−0.3 °C ky^{-1}). Over most of the SH the differences in PIG and LIG warmest-month temperature trends (WMTTs) are small. The comparison of PIG and LIG coldest-month temperature trends (CMTTs) again reveals a more complicated pattern. While in the LIG a strong cooling is simulated over the Arctic (~−0.4 °C ky^{-1}) there is no such pattern in the PIG. Furthermore, warming trends are simulated over the NH continents for both the PIG and the LIG, but

they extent further northward in the PIG while the magnitude of the warming trend in the low latitude regions is larger in the LIG. For parts of the North Atlantic and Greenland the sign of the CMTT is even opposite between the PIG (warming) and LIG (cooling). The corresponding model spread shows that the inter-model differences in the PIG temperature trends are fairly small while they tend to be larger for the LIG (Fig. 4).

In a recent study, Lohmann et al. (2013) presented multi-millennial trends in SSTs over the past 6 ky in a transient simulation with the ECHO-G GCM. We find overall a good agreement
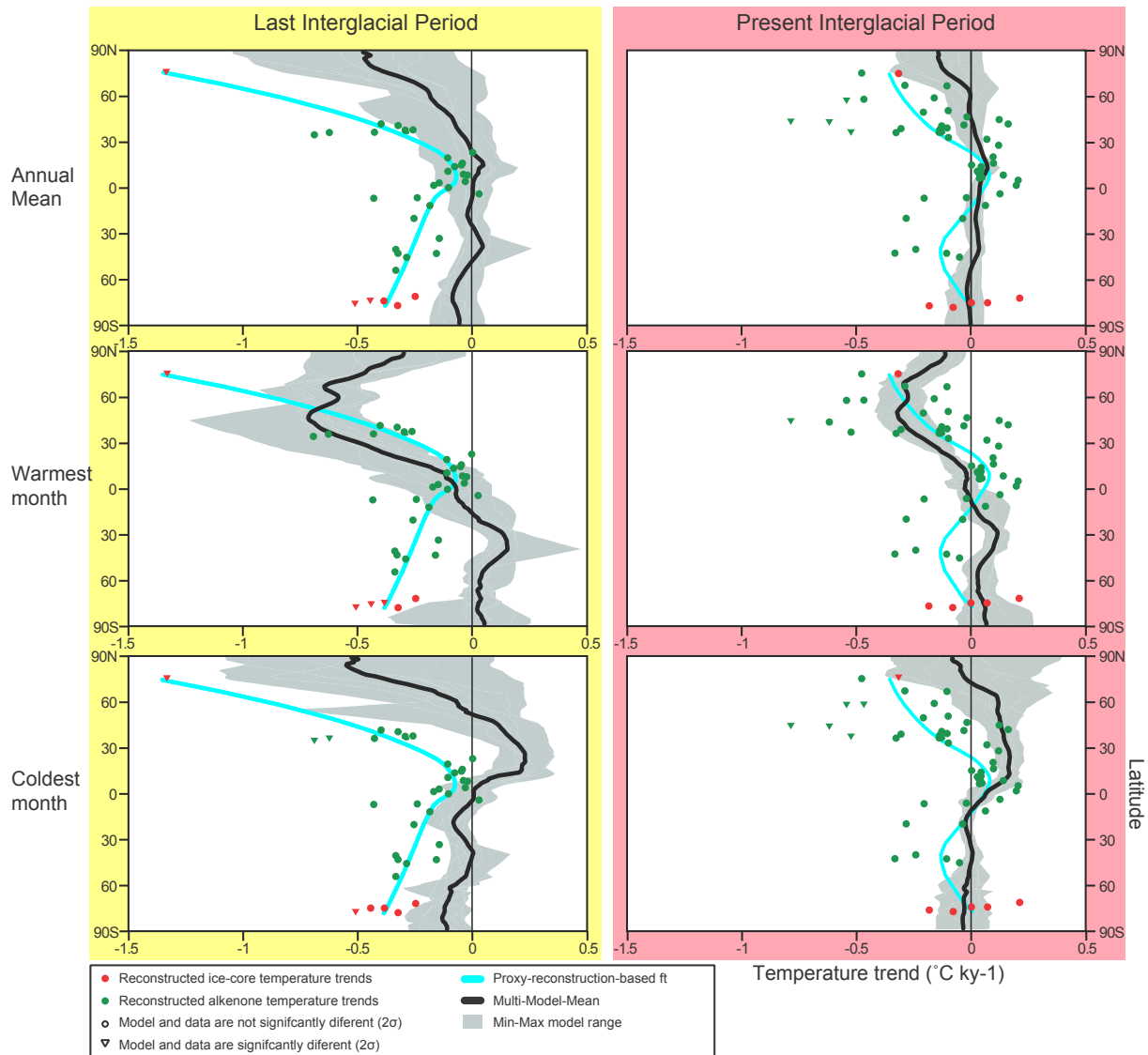
Fig. 6. Latitudinal PIG and LIG temperature trends in models and data. Model-data comparison of multi-millennial temperature trends (°C ky^{-1}) as a function of latitude for the PIG (right panel) and the LIG (left panel). From top to bottom the simulated trends are given for the: annual mean temperature trends (AMTT), warmest-month temperature trends (WMTT) and coldest-month temperature trends (CMTT; thick black lines). The given inter-model spread in this figure is not the standard deviation amongst the models but the maximum and minimum trend found in the individual model simulations (grey shading). Note that the simulated latitudinal means are averages over both continental and oceanic sites and only include grid cells for which a consistent multi-model-mean (MMM) temperature trend is found. The Greenland and Antarctic ice-core-based temperature trends reconstructions are given in red and the alkenone-based temperature trends in green. A locally weighted scatter plot smoothing (lowess) of the alkenone and ice-core based temperature trend reconstructions is shown (blue dotted lines) to indicate the general latitudinal trends and to provide a better comparison of proxy-based temperature trends with simulated longitudinal averages. Importantly, the calculations of the *t*-test statistics for the model-data comparison, included in this figure by the circle and triangle shaped symbols, is identical to Fig. 5, and thus performed locally and not against the depicted latitudinal mean MMM temperature trends. (For interpretation of the references to colour in this figure legend, the reader is referred to the web version of this article.)

between the MMM PIG trends discussed in this manuscript and the present interglacial temperature trends presented by Lohmann et al. (2013), both for annual mean, warmest and coldest months. However, a direct comparison is not straightforward because of differences in the definition of the PIG interval, because Lohmann et al. (2013) present SSTs where in this manuscript we focus on near-surface-air temperatures and because in our MMM trends, regional features are more likely to be averaged out.

3.2. Reconstructed temperature trends

Based on the reconstructed temperature time-series we have calculated PIG and LIG temperature trends over the defined target intervals. Note that the temperature trends are linear fits over a time interval which is closest to the target intervals taking into account uncertainties in the chronology and data availability. The PIG trends in the mid-to-high latitudes of the NH are ~−0.3 °C ky^{-1} (in both alkenone and Greenland ice core data), at the low latitudes slightly positive (~+0.1 °C ky^{-1}), at the mid latitudes of the SH again slightly negative (~−0.1 °C ky^{-1}) while for Antarctica ice core based temperature trends close to zero are reconstructed (Fig. 5). Regional differences appear to be especially large in the mid-to-high latitudes of the NH.

Generally the reconstructed LIG trends are larger than the PIG trends. Greenland ice-core-based temperature trends reveal a strongly negative trend (~−1.5 °C ky^{-1}), while trends of around

$\sim$$-0.5$ °C ky^{-1} are reconstructed for the mid latitudes of the NH, $\sim$$-0.2$ °C ky^{-1} at the low latitudes and $\sim$$-0.3$ °C ky^{-1} at the mid-to-high latitudes of the SH. A final remark about the reconstructed temperature trends relates to the latitudinal dependency. NH PIG and LIG as well as SH LIG alkenone and ice-core-based temperature trends reveal overall agreement, arguing for a poleward increase of the magnitude of the cooling trend. But SH PIG trends reveal a clear disagreement between alkenone and ice-core-based reconstructions because the East Antarctic ice-core-based trends are clearly smaller than the alkenone-based trends from the lower latitudes (Figs. 5 and 6).

3.3. Comparing reconstructed and simulated temperature trends

We have combined simulated and reconstructed temperature time-series for the PIG and LIG to investigate the interglacial temperature trends (see Fig. 5 for methodological details). Because the seasonality of the reconstructed temperature trends is debated and probably strongly depends on the geographical location (Leduc et al., 2010; Schneider et al., 2010), we compare the reconstructed trends with simulated annual mean, warmest month and coldest month MMM trends.

There are numerous aspects of the temperature trends that are common to both models and data (Figs. 5 and 6): *i*) In both the PIG and the LIG, AMTTs and CMTTs become more negative from the equator to the North Pole and WMTTs show maximum negative trends at NH mid latitudes and slightly positive trends in the SH, *ii*) In both the PIG and the LIG, the temperature trends in the high northern latitudes are larger than those for the high southern latitudes and finally, *iii*) the trends are overall more negative in the LIG than they are in the PIG.

The model-data comparison reveals that at more than 90% of the sites the simulated and reconstructed temperature trends are not significantly different (based on a *t*-test at 5% probability), regardless of the investigated season or interglacial period (Fig. 5). Notwithstanding, it appears from Fig. 5 that often the reason that they are not significantly different is not because there is such a good correspondence between simulated and reconstructed temperature trends. This in fact arises because both the spread amongst the models and the uncertainty in the reconstructions is relatively large (Fig. 4 and Table A1 respectively). Despite this lack of significant differences between seasons or periods, we deem that the model-data comparison allows us to describe some apparent patterns in the differences between model and data. Nonetheless, future research is needed to test the robustness of the model-data comparison outcomes discussed in the remainder of this manuscript. On a regional scale we find that the model-data comparison does improve when simulated temperatures from a particular season are used instead of annual means. A closer look at the dependence of the model-data differences on seasonality and latitude reveals some consistent patterns. For both the PIG and the LIG and independent of model complexity, the high- and mid-latitudes of the NH show a better fit between models and data if simulated WMTTs are used for the comparison instead of AMTTs (Fig. 6 and Appendix Fig. A.1). Over Greenland the magnitude of the simulated LIG WMTTs still clearly falls short of those reconstructed from ice-core data (Fig. 6). In the NH equatorial regions (0–30°N), the model-data comparison is best for AMTTs and clearly deteriorates when comparing with either simulated warmest- or coldest-month temperature trends. In contrast, in the SH equatorial region the model-data fit is unaltered regardless of which simulated temperatures are used. For the mid-to-high latitudes of the SH the model-data comparison of PIG and LIG temperature trends is very similar for AMTTs and CMTTs but deteriorates if WMTTs are used (Appendix Fig. A.1). We do note that for the SH the results are

not as consistent as they are for the NH and differences are found between the PIG and the LIG and between the EMICs and GCMs.

The improvement in the model-data agreement when seasonal rather than annual mean simulated temperature trends are considered is consistent with known seasonal biases in the response of the proxies used here (Schneider et al., 2010; Laepple et al., 2011) and broadly in accordance with the spatial differences in the seasonality effect described by Lohmann et al. (2013). We stress that the improved model-data comparison for seasonal model outputs does not necessarily indicate a seasonal bias in the proxy-records because it could be related to limitations of the climate models or their forcings, making a particular model-data comparison appear less wrong. Finally we can state that, with the exception of the temperature trends reconstructed from PIG Antarctic ice-core data, for both interglacials, SH mid-to-high latitude temperature trends are consistently more negative than the MMM results, regardless of the season (Fig. 6).

In a number of regions the different models simulate a consistent temperature trend that cannot be identified in the reconstructed temperature trends, either because the different reconstructed trends from a single region differ in sign or because there is no proxy-data coverage over these regions. Reconstructed temperature time-series from these specific regions could yield important information about the sensitivity of these climate models to changes in insolation and/or the degree of realism with which models represent climate feedbacks. An example is the Arctic Ocean where the simulations show, though with a large inter-model spread, coldest-month temperature trends that differ largely between the PIG and the LIG. Other examples are the NH continents where strong negative warmest-month temperature trends are simulated for both the PIG and the LIG, and the Sahel and Indian monsoon regions for which a majority of the models agree on a positive temperature trend in AMTT and CMTT. These patterns have been described previously for the PIG by Liu et al. (2007) and the LIG by Bakker et al. (2013).

Overall we can state that the PIG model results match the data reasonably well while the LIG model-data comparison reveals larger differences for the mid-to-high latitude regions of both hemispheres. While the proxy interpretations can be challenged because of a number of proxy shortcomings and limitations (Section 2.3), we focus hereafter on model deficiencies that could explain the model-data differences: *i*) oversimplification made in the resolution and complexity of the climate models or *ii*) missing mechanisms and feedbacks in the models.

The resolution and complexity of the models in this intercomparison differ widely. However, since we do generally find consistent temperature trends amongst the models, the limited spatial resolution and simplified physics and dynamics of the included EMICs is not likely to be the main cause of major model-data differences at the hemispheric or global scale (see also Appendix Fig. A.1). Nonetheless, at a more regional scale model-data mismatches can be related to the relatively low resolution of several models in this inter-comparison, because the models simulate temperature changes at spatial scales of at least several hundreds of kilometres while proxy reconstructions often provide a more localised signal. This mismatch in spatial scale might explain why the models cannot resolve the large regional differences in reconstructed temperature trends along, for instance, the west coast of North America and the east coast of Japan. The resolution difference between models and data provides an important argument to focus on longitudinal averages rather than regional temperature trends (Fig. 6).

Model-data differences can also be related to feedbacks from components of the climate system that are missing from the simulations. Probably the most important are the ice sheets with

related changes in the ice-sheet topography, albedo and fluxes of freshwater between the ice sheets and the oceans. For the PIG, sea-level reconstructions indicate that before ~7 ka remnants of glacial ice sheets were still present on the NH continents (Lambeck and Chappell, 2001) and still influenced the climate in specific regions (Renssen et al., 2009). But their climatic impact during this period is likely confined to small and mostly continental regions since relatively stable NH extra-tropical temperatures between 8 ka and 7 ka have been reconstructed (Marcott et al., 2013). For the LIG interval, sea-level reconstructions are more uncertain and complex, with for instance the compilation of Kopp et al. (2009) indicating a first sea-level highstand ~124 ka, indicative of reduced ice volumes compared to present-day, followed by expansion towards present-day levels ~120 ka, a secondary sea-level highstand ~118 ka and decreasing sea levels thereafter. The melting of remnant ice sheets in the PIG and the possible ice sheet melt and growth at the end of the LIG interval could have impacted local temperatures through ice-sheet-atmosphere feedbacks and large-scale temperatures through ice-sheet-ocean-circulation feedbacks. The Greenland LIG temperature reconstruction accounts only for estimated local elevation changes (NEEM community members, 2013) and there are hints of changes in East Antarctic ice-sheet topography as well, potentially related to the differences in the trends at EDC and TALDICE (Bradley et al., 2012). The Bern3D simulation is the only one that includes changes in ice-sheet cover and related freshwater fluxes. Bakker et al. (2013) show that in the Bern3D LIG simulation this additional climate forcing results in a cooling in large parts of the NH between ~130 and 125 ka, a period that is however not included in the target interval defined here.

The second possibly important component of the climate system missing in most simulations in this inter-comparison is interactive vegetation (Kutzbach et al., 1996; Claussen et al., 1999). Nonetheless, two simulations in this inter-comparison do include a vegetation component, namely CLIMBER2 and MPI-UW. The CLIMBER2 LIG simulation does show rather different July temperatures in the high latitudes of the NH and the tropics compared to the other LIG simulations (Fig. 3) and for MPI-UW an impact of vegetation changes on the LIG-period temperature evolution has been shown previously (Schurgers et al., 2007). However, for neither CLIMBER2 or MPI-UW have the impacts of vegetation changes on multi-millennial temperature trends been established or quantified.

Additional sensitivity experiments would be necessary to investigate the possible impact of changes in the ice sheets and vegetation and whether adding these two components to the simulations would improve the model-data agreement for the PIG or the LIG.

3.4. Causes of interglacial temperature trends

We have presented the characteristics of interglacial temperature changes found in both models and reconstructions for two different interglacial periods. This has revealed some consistent spatial and temporal patterns as well as substantial differences between the models and the data. In the first part of the following discussion (Sections 3.4.1–3.4.3) we will investigate what causes the simulated temperature trends. In the second part (Section 3.4.4) we combine this information with the findings from the model-data comparison in order to describe both the possible causes of the reconstructed temperature trends and to pinpoint deficiencies in the models or the forcing scenarios, most notably changes in the major ice sheets or the MOC.

The rationale behind our approach to investigate the forcings and mechanisms of the simulated temperature trends is simple. If there is a linear and positive relation between the insolation and MMM temperature trends at a given location, this indicates that the climate dynamics are relatively straightforward. If this is not the case, the results would suggest that nonlinear processes and more complex climate dynamics are at play. We will restrict our analysis to a comparison of simulated WMTTs and the insolation trends (Laskar et al., 2004) calculated for this MMM warmest month (insolation trend in warmest month; ITWM). The argument behind this is that the relation between changes in insolation and changes in temperature are likely to be strongest in the warmest months. An earlier study based on snapshot simulations performed with a coupled ocean-atmosphere GCM depicted such behaviour, with simulated Greenland summer temperature anomalies linearly related to local summer insolation, with a slope of $+0.08$ °Cm^2 W^{-1} (Masson-Delmotte et al., 2011a). Note that, according to the models, the warmest months in the mid-to-high latitudes of the NH (SH) are always found between June and August (December and February). But for the lower latitudes the models show that there are regional differences related to the hydrological cycle and the monsoon systems which results in the warmest month varying between ocean and land areas at the same latitude. As a result of these regional differences in the warmest month, the ITWM shows large spatial contrasts (Fig. 7).

The comparison of simulated WMTTs with calculated ITWMs reveals a clear pattern. For the NH mid-to-high latitudes a positive relation is found with a clear distinction between oceanic and continental regions. No such relation, however, can be detected for the mid-to-high latitudes of the SH (Fig. 7 and Appendix Fig. A.2).

3.4.1. Northern Hemisphere mid-to-high latitudes

For the NH mid-to-high latitudes there is a strong relation between the ITWM and the WMTT, which is apparent from the larger simulated trends in the LIG relative to the PIG, consistent with insolation changes. Combining results for the PIG and the LIG suggests that warmest-month temperatures over the NH mid-to-high latitude continents (40°N−90°N) are most sensitive to insolation changes with a 1 Wm^{-2} insolation change during the warmest month leading to a 0.10 °C temperature change (Appendix Fig. A.2); in other words an insolation-trend to temperature-trend relationship of $+0.10$ °Cm^2 W^{-1} ($+0.07$ to $+0.18$ °Cm^2 W^{-1}; 1σ spread among the grid cells within this regional average). Over the NH mid-to-high latitude oceans (40°N−80°N, which excludes the Arctic Ocean) the relation is $+0.09$ °Cm^2 W^{-1} ($+0.04$ to $+0.15$ °Cm^2 W^{-1}).

These insolation-trend to temperature-trend relationships for the NH mid-to-high latitudes reveal clear differences between the oceanic and continental regions. These differences can be explained by the thermal inertia of the oceans and the negative feedback related to evaporative cooling, delaying the warmest month and decreasing the temperature change (e.g. Renssen et al., 2009). Such differences between temperature changes over land and ocean have previously been quantified for the Last Glacial Maximum, the Mid-Holocene and the Last Millennium based on a combination of simulated and reconstructed temperatures (Braconnot et al., 2012). They found an average land-ocean ratio of 1.5, indicating that temperature changes over land were 50% larger than those over the adjacent oceans. Here we quantify this land-ocean contrast by comparing the WMTTs for all continental and oceanic grid cells in the NH mid-to-high latitudes. The resulting land-ocean temperature ratios are 2.1 (1.1−4.5; 1σ-range resulting from the differences within a geographic region; see Appendix Fig. A.2 for details) and 1.8 (1.1−3.2) for the PIG and LIG respectively, with both uncertainty ranges encompassing the previous estimate of 1.5. However, there are two essential differences between the approach taken by Braconnot et al. (2012) and our approach. Firstly, Braconnot et al. (2012) used temperature anomalies from Europe and the tropical regions rather than the whole NH mid-to-high latitudes, and
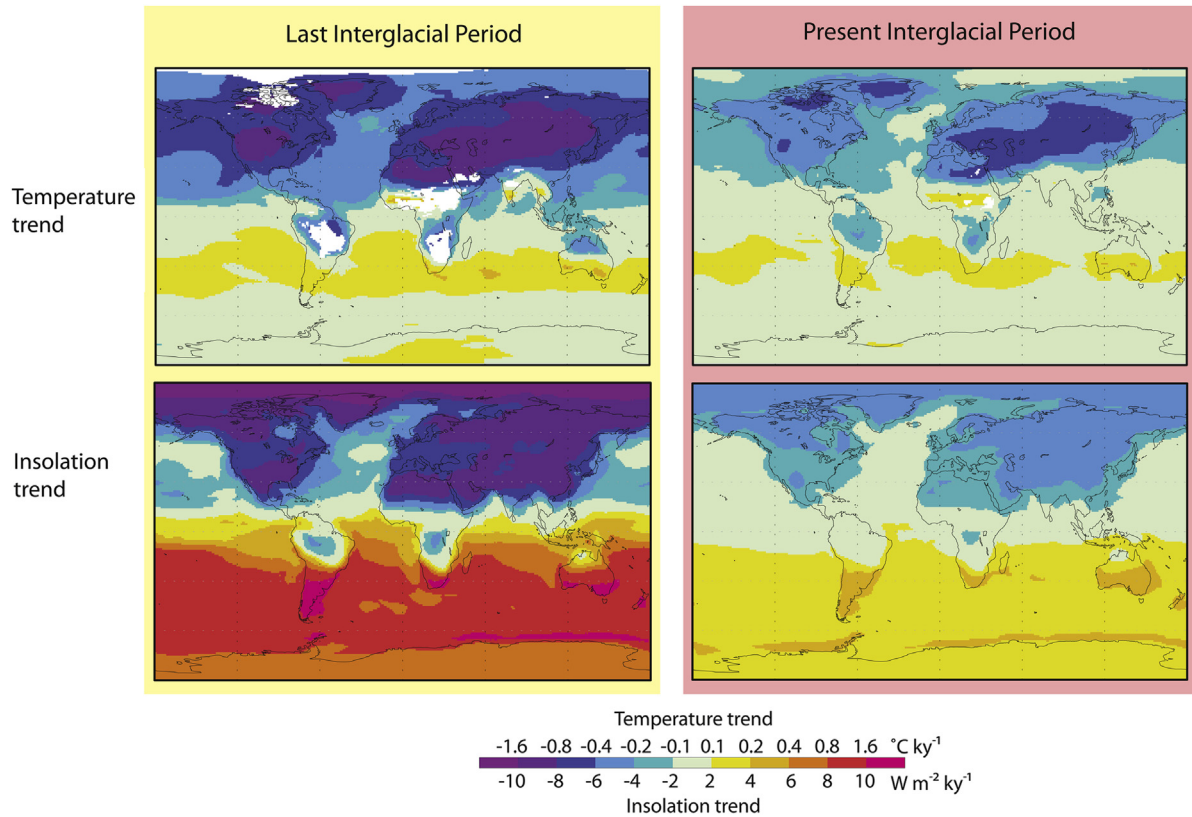
Fig. 7. Relation between PIG and LIG simulated warmest-month temperature trends and warmest-month insolation trends. Comparison of the simulated Multi-Model-Mean (MMM) temperature trends for the warmest month (WMTT) with the insolation trend for the corresponding average MMM warmest month (ITWM). The top panels show the PIG (right) and LIG (left) MMM trends ($°C$ ky^{-1}) for the warmest month as in Figs. 3 and 4. The white shading indicates that the different simulations do not give a consistent signal (see Results section for a description of the construction of the MMM temperature trends). The lower panels show the PIG and LIG insolation trend (Wm^{-2} ky^{-1}; Laskar et al., 2004) for the local average MMM warmest month.

secondly they utilised annual mean temperature anomalies rather than warmest-month temperatures. In our results, no such land-ocean ratio is found in the simulated tropical WMTTs and for annual mean temperatures from the NH mid-to-high latitudes we find land-ocean contrast ratios of 0.23—2.08 and 0.15—3.81 for the PIG and LIG respectively (see also Fig. 4 and Appendix Fig. A.2). These ranges include the previous estimate of 1.5 but also include a ratio of 1.0 which would imply that in the annual mean there is no land-ocean temperature contrast. This finding is in line with the results of Izumi et al. (2013) who show in a multi-model study of the Mid-Holocene that models agree well on the warmest month land-sea contrast, but not on an annual mean contrast. More research is needed to investigate the latitudinal and seasonal patterns of the forcings and land-sea contrasts over multi-millennial time scales and the differences between the different models.

An apparent pattern is simulated for the Arctic Ocean. While in the PIG and the in LIG the largest ITWMs are found over the Arctic Ocean, the WMTTs are not largest in this region (Fig. 7) and the relation between the temperature trend and the insolation trend is therefore smaller than for the surrounding regions with only $+0.037 °C$ m^2 W^{-1} ($+0.032$ to $+0.044 °C$ m^2 W^{-1}; Appendix Fig. A.2). This highlights the importance of the sea-ice-albedo feedback during the PIG and the LIG. However, we do note that the model spread is strikingly larger in the Arctic than it is over most other regions (Fig. 3), in line with the findings of Berger et al. (2013).

3.4.2. Low-latitudes

For the low latitudes the ITWMs are fairly small and no apparent relation is found with the simulated WMTTs (Fig. 7 and Appendix

Fig. A.2). The only exceptions are the SH low-latitude continents such as the Amazon Basin. For these regions, the results are in line with the findings for the NH mid-to-high latitudes, with a positive correlation between the insolation trends and the temperature trends of $+0.11 °C$ m^2 W^{-1} ($+0.09$ to $+0.14 °C$ m^2 W^{-1}; note that for part of the Amazon Basin no consistent multi-model signal is found). In this specific case, the ITWM is negative which can be explained by the hydrological cycle, causing the warmest month to be found in the dry winter season, in contrast to the surrounding regions.

In the Sahel and Indian monsoon areas, WMTTs seem unrelated to the ITWMs. In these regions, temperature trends result from climate feedbacks rather than directly from the small changes in the ITWM that characterise these low-latitude areas, a finding that is in line with previous modelling studies (e.g. Renssen et al., 2003). A more in-depth investigation of the LIG AMTTs (chosen here since it shows the anomalous patterns the clearest; Fig. 3) for the 9 different models in the Sahel and Indian areas indicates that the feedbacks related to monsoon dynamics are much stronger in the GCMs than they are in the EMICs (Appendix Fig. A.3). This difference results from simplifications and parameterisations of atmospheric dynamics and cloud cover in most EMICs, strongly limiting the ability to describe monsoon dynamics. Another feedback that is known to be substantial in monsoon regions is the vegetation-climate feedback (e.g. Claussen et al., 1999; Renssen et al., 2003). Interestingly, the two models that include a dynamical vegetation component (CLIMBER2 and MPI-UW) do not lie outside the range of the other simulations in these specific regions and additional sensitivity experiments are required to determine the importance
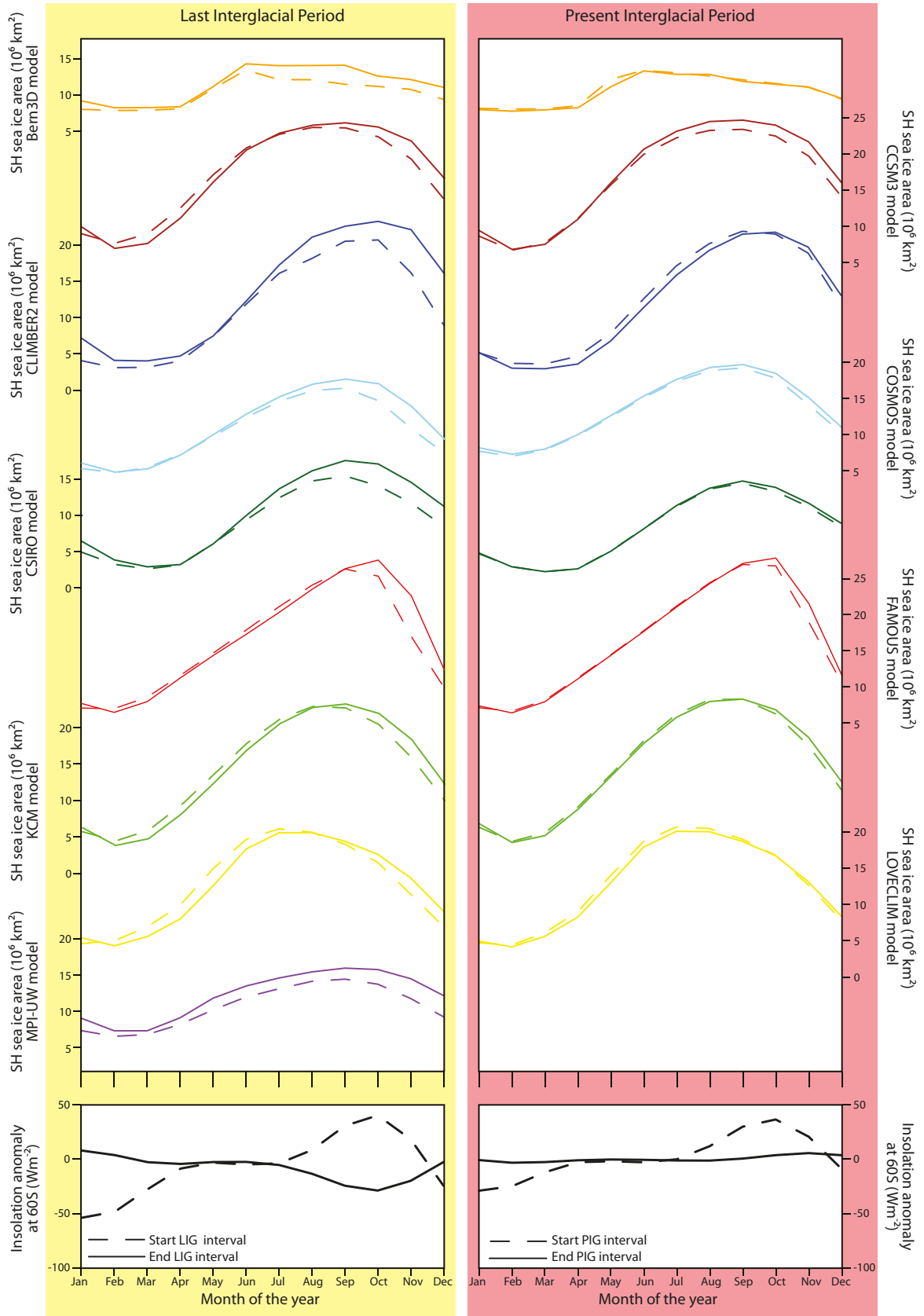
Fig. 8. PIG and LIG seasonal sea-ice area changes. Simulated seasonal cumulative SH sea-ice area (10^6 km^2) for the early and late PIG (right-hand panels) and the LIG (left-hand panels), in relation to changes in the monthly insolation (Laskar et al., 2004) anomalies with respect to 1950 AD. The values for the start of the PIG (LIG) are 250 yr averages over the 8−7.75 ka (123−122.75 ka; dashed lines) interval and over the 1.45−1.2 ka (116.45−116.2 ka; uninterrupted lines) intervals for the end of the PIG (LIG). The lower panels give the seasonal cycle of the insolation anomalies (Wm^{-2}) for both interglacial periods. For the MPI-UW model averages over 1 ky intervals were used because of the asynchronous coupling of the atmospheric component in this model. In line with the simulations, the insolation anomalies have been calculated using a fixed-day calendar.

of the climate-vegetation feedback in explaining the inter-model differences.

3.4.3. Southern Hemisphere mid-to-high latitudes

The calculated mid-to-high latitude SH ITWMs are positive and up to $+10$ Wm^{-2} ky^{-1}, only slightly smaller in magnitude than the negative trends over parts of the NH. However, in strong contrast to the NH, the simulated WMTTs over large parts of the SH are close to zero instead of clearly positive (Fig. 7). As a result, the insolation-trend to temperature-trend relationships for different SH regions are not significantly different from zero (Appendix Fig. A.2), which also indicates that even though the ITWMs during the LIG were roughly double in size compared to the PIG, the simulated WMTTs are about the same.

What causes this major contrast between the NH and the SH in the simulated temperature trends in response to insolation changes? The two main differences between the hemispheres are the ratio of continental to oceanic area and the circumpolar Southern Ocean, which has no NH counterpart. The larger ocean area in the SH yields a first-order impact on the simulated temperature trends by providing a much larger heat buffer through the large oceanic heat capacity. However, such a dampening effect cannot solely explain the simulated near zero or even negative WMTTs in response to the strongly positive ITWMs. Mechanisms are needed that counteract the direct insolation forced temperature changes by transferring insolation signals from either another season to the warmest month or from other latitudes (Renssen et al., 2005; Timmermann et al., 2009). In the following we will review different potential mechanisms identified in the literature and investigate which ones are in line with our findings. This will show that there are two mechanisms that can potentially lead to negative temperature trends: *i*) changes in the sea-ice cover have the potential to transfer the negative SH spring insolation trend into the summer season and *ii*) changes in meridional insolation gradient can change the location of the westerly winds and therewith the position of Southern Ocean upwelling areas and the related oceanic heat uptake. In addition, we will show that changes in GHG concentrations or the strength of the MOC are not responsible for counteracting the positive ITWMs in the PIG and LIG simulations.

Under the influence of changes in the astronomical forcing, spring (SON) insolation at 60°S (close to the average sea-ice edge) at the beginning of the PIG and LIG intervals is much larger than it is at the end of these intervals (changes of up to -45 Wm^{-2} for the LIG; Fig. 8). The simulations show that these negative spring insolation anomalies at the end of each interval result in an increase of the sea-ice cover during the warmest month (December according to the simulations) regardless of the warmest-month insolation increase (Fig. 8). The simulated summer austral sea-ice cover expands during the PIG by between $+1\%$ and $+14\%$ and during the LIG by between $+18\%$ and $+80\%$ (Table 2; values are relative differences between the end and start of the interglacial intervals). This increase in the summer sea-ice cover can counteract the positive ITWM by increasing the surface albedo, even though the importance of PIG and LIG SH sea-ice cover changes differs strongly amongst the models, in accordance with Roche et al. (2012) and Zunz et al. (2013). A strong relation between the evolution of SH sea ice and SH spring insolation has previously been simulated for glacial–interglacial transitions (Huybers and Denton, 2008; Timmermann et al., 2009). Now our analysis suggests that the importance of spring insolation and its impact on the evolution of SH temperatures is not restricted to glacial–interglacial transitions but is also of major importance in shaping SH temperature trends during interglacial times.

Another mechanism capable of counteracting the positive ITWMs relates to a weakening of the meridional insolation gradient. For the PIG-period, it has been shown in model inter-comparison studies with both transient and equilibrium (6 ka) simulations that in the annual mean the SH westerly winds shifted polewards over the course of the interglacial period (Rojas and Moreno, 2011; Varma et al., 2012). The latter study by Varma et al. (2012) included four simulations that are very similar to ones incorporated in this study (namely CCSM3, COSMOS, CLIMBER2 and the predecessor of LOVECLIM, ECBilt-CLIO-VECODE). We also find an increase of the strength of the westerly winds between 70°S and 50°S in most of the models, both over the PIG interval (0 to $+45\%$) and over the LIG interval (0 to $+41\%$), notwithstanding the large inter-model differences (Fig. 9 and Table 2). As a result of a poleward shift of the SH westerly winds, Varma et al. (2012) find increased upwelling of cold subsurface water in the Southern Ocean, which may induce surface atmospheric cooling. We suggest that the same mechanism described by Varma et al. (2012) for the PIG is at play during the LIG. However, upwelling in the Southern Ocean does not only depend on the strength of the overlying westerly winds but also on the vertical density structure of the ocean waters. Therefore, the impact of a wind strength increase can be counteracted by, for instance, higher surface temperatures resulting from an increase in insolation or a surface-water freshening caused by sea ice melting. The implications of changes in the latitudinal insolation gradient on SH temperatures are therefore not straightforward as is exemplified by the large inter-model differences in this study.

Table 2
Simulated changes in SH sea-ice cover and westerly-wind strength through the PIG and LIG intervals. Simulated changes in the two mechanisms that appear essential to counteract the SH warmest month insolation increases during the PIG and the LIG intervals. Columns two and three give the relative changes (%) in the cumulative SH December sea-ice area between the end and the start of the PIG and LIG intervals, respectively. Columns four and five list the simulated changes in the annual mean Southern Ocean westerly-wind strength between the end and start intervals of the PIG and LIG, respectively. The Southern Ocean is approximated by the latitude band between 70°S and 50°S. The start of the PIG (LIG) interval is defined as a 250 yr average over 8–7.75 ka (123–122.75 ka) and over the end of the PIG (LIG) interval as a 250 yr average over 1.45–1.2 ka (116.45–116.2 ka). For the MPI-UW model averages over 1 ky intervals were used because of the asynchronous coupling of the atmospheric component in this model. Note that for a number of simulations the data is not available (NA). The last row gives the multi-model-mean value and the model spread (1σ).

| Model	PIG SH Dec. sea ice area changes	LIG SH Dec. sea ice area changes	PIG Southern Ocean westerly wind changes	LIG Southern Ocean westerly wind changes
Bern3D	$+1\%$	$+18\%$	NA	NA
CCSM3	$+14\%$	$+21\%$	NA	NA
CLIMBER2	$+11\%$	$+80\%$	0%	0%
COSMOS	$+8\%$	$+27\%$	$+3\%$	$+1\%$
CSIRO	$+1\%$	$+33\%$	$+45\%$	$+31\%$
FAMOUS	$+11\%$	$+25\%$	$+1\%$	$+15\%$
KCM	$+10\%$	$+23\%$	30%	$+41\%$
LOVECLIM	$+7\%$	$+30\%$	0%	$+1\%$
MPI-UW	NA	$+32\%$	NA	$+38\%$
Mean $\pm\sigma$	7.9 ± 4.7	32.1 ± 18.6	13.2 ± 19.5	18.1 ± 18.3
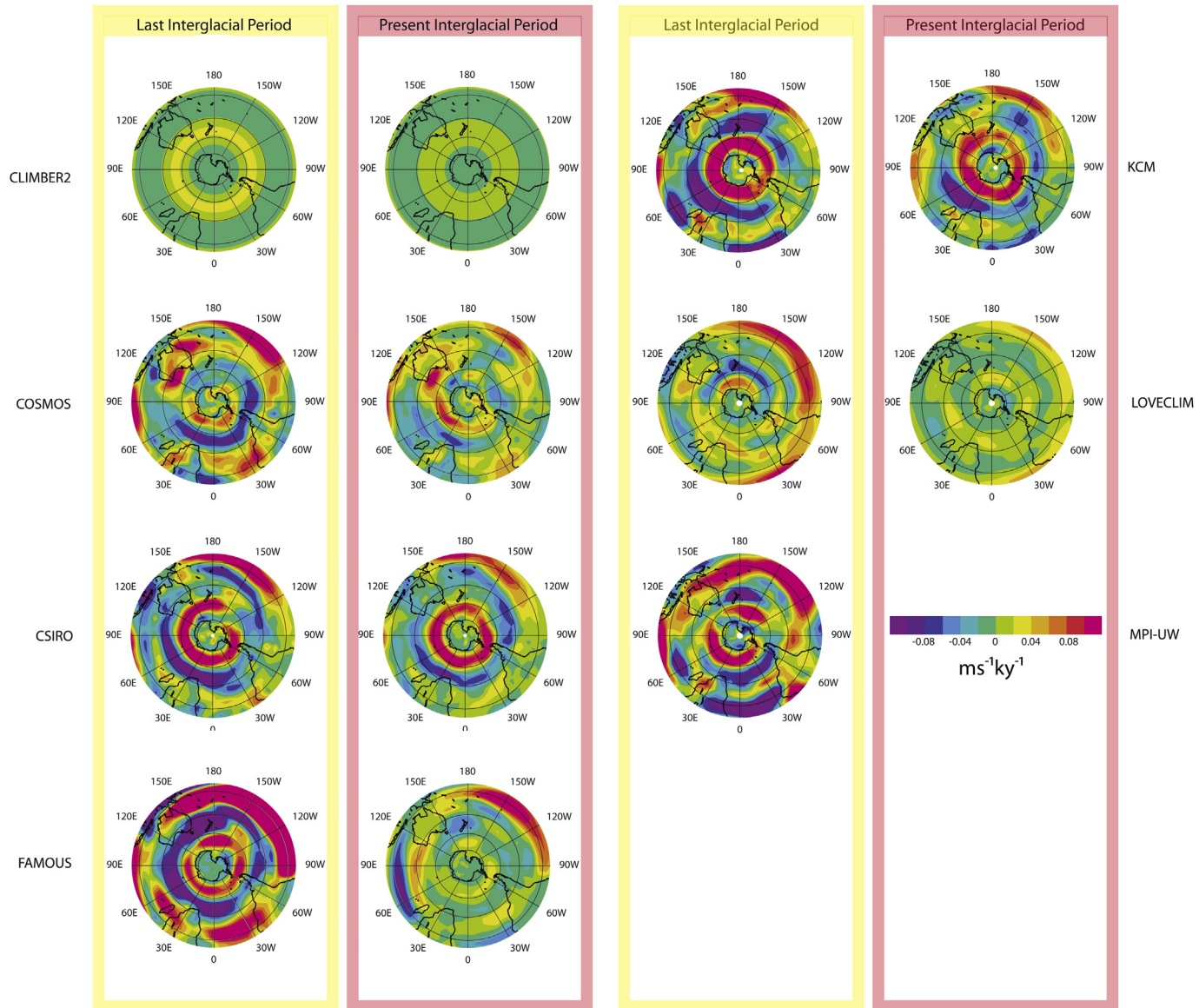
Fig. 9. PIG and LIG Southern Hemisphere annual mean zonal wind changes. Simulated changes in the annual mean SH zonal surface wind patterns (ms^{-1} ky^{-1}) through the PIG and the LIG. PIG (LIG) changes are calculated from simulated differences between the 8–7.75 ka (123–122.75 ka) and the 1.45–1.2 ka (116.45–116.2 ka) intervals. For the MPI-UW model averages over 1 ky intervals were used because of the asynchronous coupling of the atmospheric component in this model. The latitude contours in the polar stereographic plots are placed at 20° intervals, from 20°S to 80°S. The Bern3D model output is not included because the model design does not allow shifts in the location of the Westerly Winds.

Another possible impact of the decrease in the meridional insolation gradient during both the PIG and the LIG intervals has been proposed by Vimeux et al. (2001) and deals with a reduction of the poleward atmospheric moisture transport that could in turn decrease the associated heat transport and therewith counteract the positive local ITWMs. It remains unclear if such a mechanisms can explain the large difference in the simulated WMTTs between the NH and the SH, and unfortunately we do not have the appropriate model output to address this question.

A number of other mechanisms have been proposed to explain SH interglacial temperature trends, such as changes in GHG concentration changes or teleconnections between the NH and the SH (Huybers, 2009). GHG concentration changes over the time intervals under consideration are not likely to be essential in explaining the simulated WMTTs (Fig. 8), because the trends in the reconstructed GHG concentrations are slightly positive or near zero for the PIG and the LIG respectively. Moreover, the applied GHG

forcings differs largely between the different simulations and does therefore not provide an explanation for the consistency in the simulated SH temperature trends. Changes in the MOC play a key role in inter-hemispheric teleconnections that involve energy transport between the SH and the NH, such as the bipolar seesaw (Broecker, 1998). But Bakker et al. (2013) showed that (for a subset of the simulations included here) the LIG evolution of the MOC strength appears strongly model-dependent, with increases (Bern3D and FAMOUS), decreases (CLIMBER2 and LOVECLIM) or relatively stable behaviour (CCSM3, KCM and MPI-UW). These strongly differing trends in the simulated LIG MOC strength make it an unlikely explanation of the near-zero SH WMTTs consistently simulated by the different models. A potentially important issue in a future comparison of the PIG and LIG MOC evolution in models and data is the acceleration technique applied in most of the included GCM simulations. By accelerating the applied external forcings and shortening the simulation length, changes in the

circulation of the deep ocean are less likely to be realistically captured because of its long response time. This might in turn explain the apparent stability of the MOC in GCMs compared to EMICs (Bakker et al., 2013).

3.4.4. Causes of differences between simulated and reconstructed temperature trends

The climate models in this study consistently show that the negative WMTTs in the NH are driven by negative ITWM while in the SH the positive ITWMs lead to near-zero WMTTs (Fig. 7). The most substantial mechanisms to counteract the positive SH ITWMs are likely an enhanced SH spring and summer sea-ice cover and changes in Southern Ocean upwelling. The inter-model differences in the sign of the resulting WMTTs can result from slight differences in the balance between these two mechanisms and the ITWM. Furthermore, this balance can explain why the WMTTs become more negative towards the south because the centre of action of the two counteracting mechanisms is at mid-to-high SH latitudes. A final argument in favour of a balance between these two mechanisms and the ITWMs is the fact that the magnitude of the ITWMs, the changes in the latitudinal insolation gradient and the spring insolation trends were larger during the LIG than during the PIG. However, caution should be taken when assigning an important role in forcing the SH climate to obliquity changes because we based the definition of the interglacial intervals on the alignment of the climatic precession signal.

The above is a description of the mechanisms operating within the modelling realm. In contrast to the simulated near zero SH temperature trends, alkenone- and ice-core records from the SH mid-to-high latitudes consistently show negative temperature trends for both the PIG and the LIG. The exception is formed by East Antarctic PIG ice-core records that show some scattering around a near zero average trend, but note that some West Antarctic PIG ice-core records do point to local cooling (Mulvaney et al., 2012). This SH model-data mismatch in temperature changes has been shown in previous studies (Overpeck et al., 2006; Holden et al., 2010; Masson-Delmotte et al., 2010a; all focussing more on the first part of the LIG) but none of the models can capture the bipolar symmetric cooling during the second part of the LIG.

The wealth of temperature reconstructions and climate simulations combined here allows us to discuss the causes of the model-data mismatch in SH WMTTs. Firstly, it could be that models do not correctly simulate the response to increasing summer insolation and the compensatory mechanisms related to changes in climatic precession and obliquity as discussed above: increasing summer sea-ice cover caused by decreasing spring insolation and an overall increase in Southern Ocean upwelling resulting from an increase in the meridional insolation gradient. The vast majority of climate models also fail to correctly reproduce the recent trends in Southern Ocean sea ice cover (Zunz et al., 2013), supporting the hypothesis that they do not capture correctly the balance of processes in response to external and anthropogenic forcings. Nonetheless, a second option is that crucial mechanisms are missing in the simulations such as ice-sheet-MOC feedbacks. The larger scale of glaciation during the glacial period preceding the LIG-period compared to the glacial period preceding the PIG-period, potentially had a longer lasting impact on LIG-period temperatures, relative to the PIG-period (Bauch, 2013). Moreover, based on sea-level reconstructions it has been proposed that during the early to middle part of the LIG the Antarctic and/or the Greenland Ice Sheets lost substantial volumes of ice (Kopp et al., 2009; Bradley et al., 2012; NEEM community members, 2013). The SH LIG temperature trend may therefore result from an adjustment from an initial state with a different MOC configuration which is not well represented in the simulations. Melting of the Greenland Ice Sheet

is said to have led to a slowdown of the MOC during the LIG (Sánchez-Goñi et al., 2012; Govin et al., 2012). The associated bipolar see-saw mechanism is expected to have produced SH warming (Duplessy et al., 2007; Masson-Delmotte et al., 2010a) and consequently more negative WMTTs during the LIG interval. However, a slowdown of the MOC could also induce a cooling of the Southern Ocean through an advective connection (Renssen et al., 2010). Another explanation of the reconstructed LIG sea level is related to a collapse of the West Antarctic Ice Sheet which could result in an Antarctic warming via changes in the atmospheric circulation (Cuffey et al., 2006; Otto-Bliesner et al., 2006; Holden et al., 2010) or in a regional cooling because of the associated meltwater pulse into the Southern Ocean (Clark et al., 2002; Swingedouw et al., 2009). All of the above mentioned mechanisms affect the evolution of the MOC during the early part of the LIG interval. However, a cooling during the later part of the LIG interval caused by a reorganisation of the ocean circulation as part of the succeeding glacial inception provides another possible mechanism explaining the LIG SH model-data mismatch (Govin et al., 2009). It is thus clearly still an open debate as to why and how the SH and NH ice-sheet topographies together with the strength of the MOC and the related inter-hemispheric heat transport evolved over the course of the LIG, and how they could be connected to the observed bipolar cooling trends.

4. Summarising and concluding remarks

From the comparison of a large number of reconstructed and simulated temperature time-series for the PIG and the LIG intervals (8–1.2 ka and 123–116.2 ka respectively) we find overall agreement on a negative NH warmest-month temperature trend in both intervals. The simulated warmest-month temperature trends appear linearly related to the warmest-month insolation trends and to changes in climatic precession, with the same positive relation at different NH extra-tropical latitudes and for both the LIG and PIG. Notwithstanding, none of the models is able to capture the magnitude of Greenland LIG cooling recently estimated from the NEEM ice-core data. For the low latitudes, the simulated near-zero trends (in all seasons) are in agreement with alkenone trends. There are two NH regions for which large inter-model differences reveal a central role for local feedback mechanisms: the Arctic Ocean and the monsoon regions. A comparison with data for these regions would be very promising but cannot be made with the available data.

In the extra-tropical latitudes of the SH, we report a clear model-data mismatch. For both the PIG and the LIG, models show near zero SH temperature trends while negative temperature trends are found in the data. Moreover, neither the reconstructed or simulated warmest-month temperature trends adhere to a positive linear relation with warmest-month insolation changes. We argue that in both the PIG and the LIG simulations a combination of two feedback mechanisms counteract the SH warmest-month insolation increase: *i)* a decrease of the spring and summer sea-ice cover and *ii)* the upwelling of relatively cooler Southern Ocean waters as a result of a southward shift of the SH westerly winds. Deficiencies in the simulated balance between these two mechanisms and summer insolation changes could explain the model-data differences. Feedbacks not accounted for in our simulations such as ice-sheet-MOC feedbacks may however also explain the reconstructed negative temperature trends. Despite the fact that past interglacial periods are not direct analogues for future climate change, we stress the need to investigate the sensitivity of SH sea ice and Southern Ocean upwelling to seasonal and latitudinal insolation changes in climate models, as our findings question the suitability of climate models for projections in this area. Finally, our model-data

comparison relies on the classical interpretation of alkenone and ice-core stable isotope records. Improved model-data comparison techniques such as the use of models which simulate stable water isotopes would allow more effective use of the palaeoclimate information by facilitating a direct comparison between model and proxy.

Acknowledgements

Appendix A. Supplementary data

Supplementary data related to this article can be found at http://dx.doi.org/10.1016/j.quascirev.2014.06.031.

References

Andersen, K., Azuma, N., Barnola, J.M., Bigler, M., Biscaye, P., Caillon, N., Chappellaz, J., Clausen, H.B., Dahl-Jensen, D., Fischer, H., Flückiger, J., Fritzsche, D., Fujii, Y., Goto-Azuma, K., Grønvold, K., Gundestrup, N.S., Hansson, M., Huber, C., Hvidberg, C.S., Johnsen, S.J., Jonsell, U., Jouzel, J., Kipfstuhl, S., Landais, A., Leuenberger, M., Lorrain, R., Masson-Delmotte, V., Miller, H., Motoyama, H., Narita, H., Popp, T., Rasmussen, S.O., Raynaud, D., Rothlisberger, R., Ruth, U., Samyn, D., Schwander, J., Shoji, H., Siggard-Andersen, M.L., Steffensen, J.P., Stocker, T., Sveinbjörnsdóttir, A.E., Svensson, A., Takata, M., Tison, J.L., Thorsteinsson, T., Watanabe, O., Wilhelms, F., White, J.W.C., 2004. High-resolution record of Northern Hemisphere climate extending into the last interglacial period. Nature 431 (7005), 147–151.
Bakker, P., Stone, E.J., Charbit, S., Gröger, M., Krebs-Kanzow, U., Ritz, S.P., Varma, V., Khon, S., Lunt, D.J., Mikolajewicz, U., Prange, M., Renssen, H., Schneider, B., Schulz, M., 2013. Last interglacial temperature evolution – a model intercomparison. Clim. Past 9, 605–619.
Bauch, H., 2013. Interglacial climates and the Atlantic meridional overturning circulation: is there an Arctic controversy? Quat. Sci. Rev. 63, 1–22.
Bazin, L., Landais, A., Lemieux-Dudon, B., Toyé Mahamadou Kele, H., Veres, D., Parrenin, F., Martinerie, P., Ritz, C., Capron, E., Lipenkov, V., Loutre, M.-F., Raynaud, D., Vinther, B., Svensson, A., Rasmussen, S.O., Severi, M., Blunier, T., Leuenberger, M., Fischer, H., Masson-Delmotte, V., Chappellaz, J., Wolff, E., 2012. An optimized multi-proxy, multi-site Antarctic ice and gas orbital chronology (AICC2012): 120-800 ka. Clim. Past Discuss. 8, 5963–6009.
Berger, A.L., 1978. Long-term variations of caloric insolation resulting from the earth's orbital elements. Quat. Res. 9 (2), 139–167.
Berger, A., Loutre, M.F., 1991. Insolation values for the climate of the last 10 million years. Quat. Sci. Rev. 10 (4), 297–317.
Berger, M., Brandefelt, J., Nilson, J., 2013. The sensitivity of the Arctic sea ice to orbitally induced insolation changes: a study of the mid-Holocene Paleoclimate Modelling Intercomparison Project 2 and 3 simulations. Clim. Past 9, 969–982.
Braconnot, P., Otto-Bliesner, B., Harrison, S., Joussaume, S., Peterchmitt, J.-Y., Abe-Ouchi, A., Crucifix, M., Driesschaert, E., Fichefet, T., Hewitt, C.D., Kageyama, M., Kitoh, A., Laîné, A., Loutre, M.-F., Marti, O., Merkel, U., Ramstein, G., Valdes, P., Weber, S.L., Yu, Y., Zhao, Y., 2007. Results of PMIP2 coupled simulations of the Mid-Holocene and Last Glacial Maximum – part 1: experiments and large-scale features. Clim. Past 3, 261–277.
Braconnot, P., Harrison, S.P., Kageyama, M., Bartlein, P.J., Masson-Delmotte, V., Abe-Ouchi, A., Otto-Bliesner, B., Zhao, Y., 2012. Evaluation of climate models using palaeoclimatic data. Nat. Clim. Change 2 (6), 417–424.
Bradley, S.L., Siddall, M., Milne, G.A., Masson-Delmotte, V., Wolff, E., 2012. Combining ice core records and ice sheet models to explore the evolution of the East Antarctic Ice sheet during the Last Interglacial period. Glob. Planet Change 100, 278–290.

Brassell, S.C., Eglinton, G., Marlowe, I.T., Pflaumann, U., Sarnthein, M., 1986. Molecular stratigraphy: a new tool for climatic assessment. Nature 320, 129–133.
Broecker, W.S., 1998. Paleocean circulation during the Last Deglaciation: a bipolar seesaw? Paleoceanography 13, 119–121.
CAPE Last Interglacial Project Members: Anderson, P., Bennike, O., Bigelow, N., Brigham-Grette, J., Duvall, M., Edwards, M., Fréchette, B., Funder, S., Johnsen, S., Knies, J., Koerner, R., Lozhkin, A., MacDonald, G., Marshall, S., Matthiessen, J., Miller, G., Montoya, M., Muhs, D., Otto-Bliesner, B., Overpeck, J., Reeh, N., Sejrup, H. P., Turner, C., Velichko, A., 2006. Last Interglacial Arctic warmth confirms polar amplification of climate change. Quat. Sci. Rev. 25 (13–14), 1383–1400.
Clark, P.U., Mitrovica, J.X., Milne, G.A., Tamisiea, M.E., 2002. Sea-level fingerprinting as a direct test for the source of global meltwater pulse IA. Science 295, 2438–2441.
Claussen, M., Kubatzki, C., Brovkin, V., Ganopolski, A., Hoelzmann, P., Pachur, H.J., 1999. Simulation of an abrupt change in Saharan vegetation in the Mid-Holocene. Geophys. Res. Lett. 26, 2037–2040.
Collins, W.D., Bitz, C.M., Blackmon, M.L., Bonan, G.B., Bretherton, C.S., Carton, J.A., Chang, P., Doney, S.C., Hack, J.J., Henderson, T.B., Kiehl, J.T., Large, W.G., McKenna, D.S., Santer, B.D., Smith, R.D., 2006. The community climate system model version 3 (CCSM3). J. Clim. 19, 2122–2143.
Conte, M.H., Sicre, M.A., Rühlemann, C., Weber, J.C., Schulte, S., Schulz-Bull, D., Blanz, T., 2006. Global temperature calibration of the alkenone unsaturation index (UK37) in surface waters and comparison with surface sediments. Geochem. Geophys. Geosyst. 7, Q02005. http://dx.doi.org/10.1029/2005gc001054.
Duplessy, J.C., Roche, D.M., Kageyama, M., 2007. The deep ocean during the Last Interglacial period. Science 316 (5821), 89–91.
Edwards, N.R., Marsh, R., 2005. Uncertainties due to transportparameter sensitivity in an efficient 3-D ocean-climate model. Clim. Dyn. 24, 415–433.
Epstein, B.L., D'Hondt, S., Hargraves, P.E., 2001. The possible metabolic role of C37 alkenones in Emiliania huxleyi. Org. Geochem. 32, 867–875.
Goosse, H., Brovkin, V., Fichefet, T., Haarsma, R., Huybrechts, P., Jongma, J., Mouchet, A., Selten, F., Barriat, P.-Y., Campin, J.-M., Deleersnijder, E., Driesschaert, E., Goelzer, H., Janssens, I., Loutre, M.-F., Morales Maqueda, M.A., Opsteegh, T., Mathieu, P.-P., Munhoven, G., Pettersson, E.J., Renssen, H., Roche, D.M., Schaeffer, M., Tartinville, B., Timmermann, A., Weber, S.L., 2010. Description of the Earth system model of intermediate complexity LOVECLIM version 1.2. Geosci. Model Dev. 3, 603–633.
Gordon, C., Cooper, C., Senior, C.A., Banks, H., Gregory, J.M., Johns, T.C., Mitchell, J.F.B., Wood, R.A., 2000. The simulation of SST, sea ice extents and ocean heat transports in a version of the Hadley Centre coupled model without flux adjustments. Clim. Dyn. 16, 147–168.
Govin, A., Michel, E., Labeyrie, L., Waelbroeck, C., Dewilde, F., Jansen, E., 2009. Evidence for northward expansion of Antarctic Bottom Water mass in the Southern Ocean during the last glacial inception. Paleoceanography 24, PA1202.
Govin, A., Braconnot, P., Capron, E., Cortijo, E., Duplessy, J.C., Jansen, E., Labeyrie, L., Landais, A., Marti, O., Michel, E., Mosquet, E., Risebrobakken, B., Swingedouw, D., Waelbroeck, C., 2012. Persistent influence of ice sheet melting on high northern latitude climate during the early Last Interglacial. Clim. Past 8, 483–507.
Gröger, M., Maier-Reimer, E., Mikolajewicz, U., Schurgers, G., Vizcaíno, M., Winguth, A., 2007. Changes in the hydrological cycle, ocean circulation, and carbon/nutrient cycling during the last interglacial and glacial transition. Paleoceanography 22, PA4205.
Holden, P.B., Edwards, N.R., Wolff, E.W., Lang, N.J., Singarayer, J.S., Valdes, P.J., Stocker, T.F., 2010. Interhemispheric coupling, the West Antarctic Ice Sheet and warm Antarctic interglacials. Clim. Past 6 (4), 431–443.
Huybers, P., 2009. Antarctica's orbital beat. Science 325 (5944), 1085–1086.
Huybers, P., Denton, G., 2008. Antarctic temperature at orbital timescales controlled by local summer duration. Nat. Geosci. 1 (11), 787–792.
Izumi, K., Bartlein, P.J., Harrison, S.P., 2013. Consistent large-scale temperature responses in warm and cold climates. Geophys. Res. Lett. 40 (9), 1817–1823.
Jones, P.D., New, M., Parker, D.E., Martin, S., Rigor, I.G., 1999. Surface air temperature and its changes over the past 150 years. Rev. Geophys. 37 (2), 173–199.
Jones, P.D., Gregory, J., Thorpe, R., Cox, P., Murphy, J., Sexton, D., Valdes, P., 2005. Systematic optimisation and climate simulations of FAMOUS, a fast version of HadCM3. Clim. Dyn. 25, 189–204.
Joussaume, S., Braconnot, P., 1997. Sensitivity of paleoclimate simulation results to season definitions. J. Geophys. Res. 102, 1943–1956.
Jouzel, J., Masson-Delmotte, V., 2010. Paleoclimates: what do we learn from deep ice cores? WIREs Clim. Change 1 (5), 654–669.
Jouzel, J., Vimeux, F., Caillon, N., Delaygue, G., Hoffmann, G., Masson-Delmotte, V., Parrenin, F., 2003. Magnitude of isotope/temperature scaling for interpretation of central Antarctic ice cores. J. Geophys. Res. 108, 4361.
Kopp, R.E., Simons, F.J., Mitrovica, J.X., Maloof, A.C., Oppenheimer, M., 2009. Probabilistic assessment of sea level during the last interglacial stage. Nature 462 (7275), 863–867.
Kutzbach, J.E., Bartlein, P.J., Foley, J.A., Harrison, S.P., Hostetler, S.W., Liu, Z., Prentice, I.C., Webb, T., 1996. Potential role of vegetation feedback in the climate sensitivity of high-latitude regions: a case study at 6000 years B.P. Glob. Biogeochem. Cycles 10, 727–736.
Laepple, T., Werner, M., Lohmnann, G., 2011. Synchronicity of Antarctic temperatures and local solar insolation on orbital timescales. Nature 471 (7336), 91–94.
Lambeck, K., Chappell, J., 2001. Sea level change through the Last Glacial cycle. Science 292 (5517), 679–686.

Langebroek, P.M., Nisancioglu, K.H., 2013. Simulating last interglacial climate with NorESM: role of insolation and greenhouse gases in the timing of peak warmth. Clim. Past Discuss. 9, 4449—4473.

Laskar, J., Robutel, P., Joutel, F., Gastineau, M., Correia, A.C.M., Levrard, B., 2004. A long-term numerical solution for the insolation quantities of the Earth. Astron. Astrophys. 428 (1), 261—285.

Leduc, G., Schneider, R., Kim, J.H., Lohmann, G., 2010. Holocene and Eemian sea surface temperature trends as revealed by alkenone and Mg/Ca paleo-thermometry. Quat. Sci. Rev. 29 (7—8), 989—1004.

Liu, Z., Wang, Y., Gallimore, R., Gasse, F., Johnson, T., deMenocal, P., Adkins, J., Notaro, M., Prentice, I.C., Kutzback, J., Jacob, R., Behling, P., Wang, L., Ong, E., 2007. Simulating the transient evolution and abrupt changes of Northern Africa atmosphere—ocean—terrestrial ecosystem in the Holocene. Quat. Sci. Rev. 26 (13—14), 1818—1837.

Locarnini, R.A., Mishonov, A.V., Antonov, J.I., Boyer, T.P., Garcia, H.E., Baranova, O.K., Zweng, M.M., Johnson, D.R., 2010. In: Levitus, S. (Ed.), World Ocean Atlas 2009, Temperature, vol. 1. NOAA Atlas NESDIS 68, U.S. Government Printing Office, Washington, D.C., 184 pp.

Lohmann, G., Pfeiffer, M., Laepple, T., Leduc, G., Kim, J.-H., 2013. A model—data comparison of the Holocene global sea surface temperature evolution. Clim. Past 9, 1807—1839.

Lorenz, S.J., Lohmann, G., 2004. Acceleration technique for Milankovitch type forcing in a coupled atmosphere-ocean circulation model: method and appli-cation for the Holocene. Clim. Dyn. 23 (7—8), 727—743.

Lunt, D.J., Abe-Ouchi, A., Bakker, P., Berger, A., Braconnot, P., Charbit, S., Fischer, N., Herold, N., Jungclaus, J.H., Khon, V.C., Krebs-Kanzow, U., Langebroek, P.M., Lohmann, G., Nisancioglu, K.H., Otto-Bliesner, B., Park, W., Pfeiffer, M., Phipps, S.J., Prange, M., Rachmayani, R., Renssen, H., Rosenbloom, N., Schneider, B., Stone, E.J., Takahashi, K., Wei, W., Yin, Q., Zhang, Z.S., 2013. A multi-model assessment of last interglacial temperatures. Clim. Past 9, 699—717.

Marcott, S.A., Shakun, J.D., Clark, P.U., Mix, A.C., 2013. A reconstruction of regional and global temperature for the past 11,300 years. Science 339 (6124), 1198—1201.

Marsland, S.J., Haak, H., Jungclaus, J.H., Latif, M., Röske, F., 2003. The Max-Planck-Institute global ocean/sea ice model with orthogonal curvilinear coordinates. Ocean Modell. 5, 91—127.

Masson-Delmotte, V., Dreyfus, G., Braconnot, P., Johnson, S., Jouzel, J., Kageyama, M., Landais, A., Loutre, M.F., Nouet, J., Parrenin, F., Raynaud, D., Stenni, B., Tuenter, E., 2006. Past temperature reconstructions from deep ice cores: relevance for future climate change. Clim. Past 2 (2), 145—165.

Masson-Delmotte, V., Stenni, B., Pol, K., Braconnot, P., Cattani, O., Falourd, S., Kageyama, M., Jouzel, J., Landais, A., Minster, B., Barnola, J.M., Chappellaz, J., Krinner, G., Johnsen, S., Röthlisberger, R., Hansen, J., Mikolajewicz, U., Otto-Bliesner, B., 2010a. EPICA Dome C record of glacial and interglacial intensities. Quat. Sci. Rev. 29 (1—2), 113—128.

Masson-Delmotte, V., Stenni, B., Blunier, T., Cattani, O., Chappellaz, J., Cheng, H., Dreyfus, G., Edwards, R.L., Falourd, S., Govin, A., Kawamura, K., Johnsen, S.J., Jouzel, J., Landais, A., Lemieux-Dudon, B., Lourantou, A., Marshall, G., Minster, B., Mudelsee, M., Pol, K., Öthlisberger, R., Selmo, E., Waelbroeck, C., 2010b. Abrupt change of Antarctic moisture origin at the end of Termination. PNAS 107 (27), 12091—12094.

Masson-Delmotte, V., Braconnot, P., Hoffmann, G., Jouzel, J., Kageyama, M., Landais, A., Lejeune, Q., Risi, C., Sime, L., Sjolte, J., Swingedouw, D., Vinther, B., 2011a. Sensitivity of interglacial Greenland temperature and δ18O: ice core data, orbital and increased CO2 climate simulations. Clim. Past 7 (3), 1041—1059.

Masson-Delmotte, V., Buiron, D., Ekaykin, A., Frezzotti, M., Gallée, H., Jouzel, J., Krinner, G., Landais, A., Motoyama, H., Oerter, H., Pol, K., Pollard, D., Ritz, C., Schlosser, E., Sime, L.C., Sodemann, H., Stenni, B., Uemura, R., Vimeux, F., 2011b. A comparison of the present and last interglacial periods in six Antarctic ice cores. Clim. Past 7 (2), 397—423.

McKay, N.P., Overpeck, J.T., Otto-Bliesner, B.L., 2011. The role of ocean thermal expansion in Last Interglacial sea level rise. Geophys. Res. Lett. 38 (14), L14605.

Mikolajewicz, U., Gröger, M., Maier-Reimer, E., Schurgers, G., Vizcaíno, M., Winguth, A., 2007. Long-term effects of anthropogenic CO2 emissions simu-lated with a complex earth system model. Clim. Dyn. 28, 599—633.

Milankovitch, M., 1941. Kanon der Erdbestrahlung und seine Andwendung auf das Eiszeiten-problem. R. Serbian Acad, Belgrade.

Mulvaney, Robert, Abram, Nerilie J., Hindmarsh, Richard C.A., Arrowsmith, Carol, Fleet, Louise, Triest, Jack, Sime, Louise C., Alemany, Olivier, Foord, Susan, 2012. Recent Antarctic Peninsula warming relative to Holocene climate and ice-shelf history. Nature 489 (7414), 141—144.

Müller, P.J., Kirst, G., Ruhland, G., von Storch, I., Rosell-Melé, A., 1998. Calibration of the alkenone paleotemperature index U37K' based on core-tops from the eastern South Atlantic and the global ocean (60°N-60°S). Geochim. Cosmochim. Acta 62, 1757—1772.

Müller, S.A., Joos, F., Edwards, N.R., Stocker, T.F., 2006. Water mass distribution and ventilation time scales in a cost-efficient, three-dimensional ocean model. J. Clim. 19, 5479—5499.

NEEM community members, 2013. Eemian interglacial reconstructed from a Greenland folded ice core. Nature 493 (7433), 489—494.

Otto-Bliesner, B.L., Brady, E., Clauzet, E.C., Tomas, G., Levis, R., Zav, S.K., 2006. Last Glacial Maximum and Holocene climate in CCSM3. J. Clim. 19 (11), 2526—2544.

Overpeck, J.T., Otto-Bliesner, B.L., Miller, G.H., Muhs, D.R., Alley, R.B., Kiehl, J.T., 2006. Paleoclimatic evidence for future ice-sheet instability and rapid sea-level rise. Science 311 (5768), 1747—1750.

PALAEOSENS Project Members, 2012. Making sense of palaeoclimate sensitivity. Nature 491 (7426), 683—691.

Park, W., Keenlyside, N., Latif, M., Stroh, A., Redler, R., Roeckner, E., Madec, G., 2009. Tropical Pacific climate and its response to global warming in the Kiel climate model. J. Clim. 22, 71—92.

Parrenin, F., Barnola, J.-M., Beer, J., Blunier, T., Castellano, E., Chappellaz, J., Dreyfus, G., Fischer, H., Fujita, S., Jouzel, J., Kawamura, K., Lemieux-Dudon, B., Loulergue, L., Masson-Delmotte, V., Narcisi, B., Petit, J.-R., Raisbeck, G., Raynaud, D., Ruth, U., Schwander, J., Severi, M., Spahni, R., Steffensen, J.P., Svensson, A., Udisti, R., Waelbroeck, C., Wolff, E., 2007. The EDC3 chronology for the EPICA Dome C ice core. Clim. Past 3, 485—497.

Pelejero, C., Grimalt, J.O., 1997. The correlation between the 37k index and sea surface temperatures in the warm boundary: the South China Sea. Geochim. Cosmochim. Acta 61, 4789—4797.

Petoukhov, V., Ganopolski, A., Brovkin, V., Claussen, M., Eliseev, A., Kubatzki, C., Rahmstorf, S., 2000. CLIMBER-2: a climate system model of intermediate complexity. Part I: model description and performance for present climate. Clim. Dyn. 16, 1—17.

Phipps, S.J., Rotstayn, L.D., Gordon, H.B., Roberts, J.L., Hirst, A.C., Budd, W.F., 2011. The CSIRO Mk3L climate system model version 1.0-part 1: description and evaluation. Geosci. Model Dev. 4, 483—509. http://dx.doi.org/10.5194/gmd-4-483-2011.

Phipps, S.J., Rotstayn, L.D., Gordon, H.B., Roberts, J.L., Hirst, A.C., Budd, W.F., 2012. The CSIRO Mk3L climate system model version 1.0-part 2: response to external forcings. Geosci. Model Dev. 5, 649—682. http://dx.doi.org/10.5194/gmd-5-649-2012.

Prahl, F.G., Wakeham, S.G., 1987. Calibration of unsaturation patterns in long-chain ketone compositions for palaeotemperature assessment. Nature 330, 367—369.

Prahl, F.G., Muehlhausen, L.A., Zahnle, D.L., 1988. Further evaluation of long-chain alkenones as indicators of paleoceanographic conditions. Geochim. Cosmo-chim. Acta 52, 2303—2310.

Renssen, H., Brovkin, V., Fichefet, T., Goosse, H., 2003. Holocene climate instability during the termination of the African Humid Period. Geophys. Res. Lett. 30 (4), 1184—1187.

Renssen, H., Goosse, H., Fichefet, T., Masson-Delmotte, V., Koç, N., 2005. Holocene climate evolution in the high-latitude Southern Hemisphere simulated by a coupled atmosphere-sea ice-ocean-vegetation model. Holocene 15 (7), 951—964.

Renssen, H., Seppa, H., Heiri, O., Roche, D.M., Goosse, H., Fichefet, T., 2009. The spatial and temporal complexity of the Holocene thermal maximum. Nat. Geosci. 2 (6), 411—414.

Renssen, H., Goosse, H., Crosta, X., Roche, D.M., 2010. Early Holocene Laurentide Ice Sheet deglaciation causes cooling in the high-latitude Southern Hemisphere through oceanic teleconnection. Paleoceanography 25 (3), 15.

Ritz, S.P., Stocker, T.F., Joos, F., 2011a. A coupled dynamical ocean-energy balance atmosphere model for Paleoclimate studies. J. Clim. 24, 349—375.

Ritz, S.P., Stocker, T.F., Severinghaus, J.P., 2011b. Noble gases as proxies of mean ocean temperature: sensitivity studies using a climate model of reduced complexity. Quat. Sci. Rev. 30, 3728—3741.

Roche, D.M., Crosta, X., Renssen, H., 2012. Evaluating Southern Ocean sea ice for the Last Glacial Maximum and pre-industrial climates: PMIP-2 models and data evidence. Quat. Sci. Rev. 56, 99—106.

Rojas, M., Moreno, P., 2011. Atmospheric circulation changes and neoglacial con-ditions in the Southern Hemisphere mid-latitudes: insights from PMIP2 sim-ulations at 6 kyr. Clim. Dyn. 37 (1—2), 357—375.

Roeckner, E., Bäuml, G., Bonaventura, L., Brokopf, R., Esch, M., Giorgetta, M., Hagemann, S., Kirchner, I., Kornblueh, L., Manzini, E., Rhodin, A., Schlese, U., Schulzweida, U., Tompkins, A., 2003. The Atmospheric General Circulation Model ECHAM5. PART I: Model Description. Tech rep, Max Planck Institute for Meteorology, MPI-Report 349.

Rosell-Melé, A., Prahl, F.G., 2013. Seasonality of temperature estimates as inferred from sediment trap data. Quat. Sci. Rev. 72, 128—136.

Rosell-Melé, A., Eglinton, G., Pflaumann, U., Sarnthein, M., 1995. Atlantic core-top calibration of the U37K index as a sea-surface palaeotemperature indicator. Geochim. Cosmochim. Acta 59, 3099—3107.

Ruddiman, W.F., Vavrus, S.J., Kutzbach, J.E., 2005. A test of the overdue-glaciation hypothesis. Quat. Sci. Rev. 4, 1—10.

Rühlemann, C., Butzin, M., 2006. Alkenone temperature anomalies in the Brazil-Malvinas Confluence area caused by lateral advection of suspended particu-late material. Geochem. Geophys. Geosyst. 7, Q10015.

Sánchez-Goñi, M.F., Bakker, P., Desprat, S., Carlson, A.E., Van Meerbeeck, C.J., Peyron, O., Naughton, F., Fletcher, W.J., Eynaud, F., Rossignol, L., Renssen, H., 2012. European climate optimum and enhanced Greenland melt during the Last Interglacial. Geology 40 (7), 627—630.

Schneider, B., Leduc, G., Park, W., 2010. Disentangling seasonal signals in Holocene climate trends by satellite-model-proxy integration. Paleoceanography 25, PA4217.

Schurgers, G., Mikolajewicz, U., Gröger, M., Maier-Reimer, E., Vizcaíno, M., Winguth, A., 2007. The effect of land surface changes on Eemian climate. Clim. Dyn. 29 (4), 357—373.

Shackleton, N.J., Sánchez-Goñi, M.F., Pailler, D., Lancelot, Y., 2003. Marine Isotope Substage 5e and the Eemian Interglacial. Glob. Planet. Change 36 (3), 151—155.

Sicre, M.A., Labeyrie, L., Ezat, U., Duprat, J., Turon, J.L., Schmidt, S., Michel, E., Mazaud, A., 2005. Mid-latitude Southern Indian Ocean response to Northern Hemisphere Heinrich events. Earth Planet. Sci. Lett. 240, 724—731.

Sime, L.C., Wolff, E.W., 2011. Antarctic accumulation seasonality. Nature 479 (7372), E1—E2.

Sime, L.C., Tindall, J.C., Wolff, E.W., Connolley, W.M., Valdes, P.J., 2008. Antarctic isotopic thermometer during a CO2 forced warming event. J. Geophys. Res. 113, D24119.

Smith, R.S., 2012. The FAMOUS climate model (version XFXWB and XFHCC): description update to version XDBUA. Geosci. Model Dev. 5, 269—276.

Smith, R., Gregory, J., 2012. The last glacial cycle: transient simulations with an AOGCM. Clim. Dyn. 38, 1545—1559.

Sonzogni, C., Bard, E., Rostek, F., Lafont, R., Rosell-Mele, A., Eglinton, G., 1997. Core-top calibration of the alkenone index vs sea surface temperature in the Indian Ocean. Deep Sea Res. Part II Top. Stud. Oceanogr. 44, 1445—1460.

Stenni, B., Masson-Delmotte, V., Selmo, E., Oerter, H., Meyer, H., Röthlisberger, R., Jouzel, J., Cattani, O., Falourd, S., Fisher, H., Hoffmann, G., Iacumin, P., Johnsen, S.J., Minster, B., Udisti, R., 2010. The deuterium excess records of EPICA Dome C and Dronning Maud Land ice cores (East Antarctica). Quat. Sci. Rev. 29 (1—2), 146—159.

Swingedouw, D., Fichefet, T., Goosse, H., Loutre, M., 2009. Impact of transient freshwater releases in the Southern Ocean on the AMOC and climate. Clim. Dyn. 33 (2), 365—381.

Thierstein, H.R., Young, J.R. (Eds.), 2004. Coccolithophores from Cellular Process to Global Impact. Springer Verlag.

Timmermann, A., Timm, O., Stott, L., Menviel, L., 2009. The roles of CO2 and orbital forcing in driving southern hemispheric temperature variations during the last 21 000 yr. J. Clim. 22, 1626—1640.

Turney, C.S.M., Jones, R.T., 2010. Does the Agulhas Current amplify global temperatures during super-interglacials? J. Quat. Sci. 25 (6), 839—843.

Uemura, R., Masson-Delmotte, V., Jouzel, J., Landais, A., Motoyama, H., Stenni, B., 2012. Ranges of moisture-source temperature estimated from Antarctic ice cores stable isotope records over glacial-interglacial cycles. Clim. Past 8 (3), 1109—1125.

Varma, V., Prange, M., Merkel, U., Kleinen, T., Lohmann, G., Pfeiffer, M., Renssen, H., Wagner, A., Wagner, S., Schulz, M., 2012. Holocene evolution of the Southern Hemisphere westerly winds in transient simulations with global climate models. Clim. Past 8 (2), 391—402.

Vimeux, F., Masson-Delmotte, V., Jouzel, J., Petit, J.R., Steig, E.J., Stievenard, M., Vaikmae, R., White, J.W.C., 2001. Holocene hydrological cycle changes in the Southern Hemisphere documented in East Antarctic deuterium excess records. Clim. Dyn. 17 (7), 503—513.

Vinther, B.M., Buchardt, S.L., Clausen, H.B., Dahl-Jensen, D., Johnsen, S.J., Fisher, D.A., Koerner, R.M., Raynaud, D., Lipenkov, V., Andersen, K.K., Blunier, T., Rasmussen, S.O., Steffensen, J.P., Svensson, A.M., 2009. Holocene thinning of the Greenland ice sheet. Nature 461 (7262), 385—388.

Waelbroeck, C., Frank, N., Jouzel, J., Parrenin, F., Masson-Delmotte, V., Genty, D., 2008. Transferring radiometric dating of the last interglacial sea level high stand to marine and ice core records. Earth Planet. Sci. Lett. 265 (1—2), 183—194.

Wanner, H., Beer, J., Butikofer, J., Crowley, T.J., Cubasch, U., Fluckiger, J., Goosse, H., Grosjean, M., Joos, F., Kaplan, J.O., Kuttel, M., Muller, S.A., Prentice, I.C., Solomina, O., Stocker, T.F., Tarasov, P., Wagner, M., Widmann, M., 2008. Mid- to Late Holocene climate change: an overview. Quat. Sci. Rev. 27, 1791—1828.

Zunz, V., Goosse, H., Massonnet, F., 2013. How does internal variability influence the ability of CMIP5 models to reproduce the recent trend in Southern Ocean sea ice extent? Cryosphere 7, 451—468.